Molecular mechanisms of snoRNA-IL15 crosstalk in adipocyte lipolysis and NK cell rejuvenation

Yaohua Zhang[1,#], Zilong Zhao[1,#], Lisa A. Huang[1,#], Yuan Liu[2], Yun Yao[1], Chengcao Sun[1], Yajuan Li[1], Zhao Zhang[2], Youqiong Ye[2], Fei Yuan[3], Tina K. Nguyen[1], Nikhil Reddy Garlapati[1], Andrew Wu[1], Sergey D. Egranov[1], Abigail S. Caudle[4], Aysegul A. Sahin[5], Bora Lim[6], Laura Beretta[1], George A. Calin[7,8], Dihua Yu[1,9], Mien-Chie Hung[10,11], Michael Curran[9,12], Katayoun Rezvani[9,13], Boyi Gan[9,14], Zhi Tan[3,*], Leng Han[2,*], Chunru Lin[1,9,*], Liuqing Yang[1,8,9,15,*]

[1]Department of Molecular and Cellular Oncology, The University of Texas MD Anderson Cancer Center, Houston, TX 77030, USA

[2]Center for Epigenetics and Disease Prevention, Institute of Biosciences and Technology, Texas A&M University, Houston, TX, USA

[3]Center for Drug Discovery, Department of Pathology & Immunology, Baylor College of Medicine, Houston, TX 77030, USA

[4]Department of Breast Surgical Oncology, Division of Surgery, The University of Texas MD Anderson Cancer Center, Houston, TX 77030, USA

[5]Department of Pathology, Division of Pathology and Laboratory Medicine, The University of Texas MD Anderson Cancer Center, Houston, TX 77030, USA

[6]Oncology/Medicine, Dan L Duncan Comprehensive Cancer Center, Baylor College of Medicine, Houston, TX

[7]Department of Translational Molecular Pathology, The University of Texas MD Anderson Cancer Center, Houston, TX 77030, USA

[8]Center for RNA Interference and Non-Coding RNAs, The University of Texas MD Anderson Cancer Center, Houston, TX 77030, USA

*Correspondence: zhi.tan@bcm.edu, leng.han@tamu.edu, clin2@mdanderson.org and lyang7@mdanderson.org.
#Denotes equal contribution

[9]The Graduate School of Biomedical Sciences, The University of Texas MD Anderson Cancer Center, Houston, TX 77030, USA

[10]Graduate Institute of Biomedical Sciences, Research Center for Cancer Biology, and Center for Molecular Medicine, China Medical University, Taichung 404, Taiwan

[11]Department of Biotechnology, Asia University, Taichung 413, Taiwan

[12]Department of Immunology, The University of Texas MD Anderson Cancer Center, Houston, TX 77030, USA

[13]Department of Stem Cell Transplantation and Cellular Therapy, The University of Texas MD Anderson Cancer Center, Houston, TX, USA

[14]Department of Experimental Radiation Oncology, Division of Radiation Oncology, The University of Texas MD Anderson Cancer Center, Houston, TX 77030, USA

[15]Lead contact

Summary

Obesity, in which the functional importance of small nucleolar RNAs (snoRNAs) remains elusive, correlates with the risk for many cancer types. Here, we identify that the serum copies of adipocyte-expressed *SNORD46* correlates with body mass index (BMI) and serum *SNORD46* antagonizes interleukin-15 (IL15) signaling. Mechanically, *SNORD46* binds IL15 *via* G11 and G11A (a mutation significantly enhances binding affinity) knockin drives obesity in mice. Functionally, *SNORD46* blocks IL15-induced, FER kinase-dependent phosphorylation of platelet glycoprotein 4 (CD36) and monoglyceride lipase (MGLL) in adipocytes, leading to inhibited lipolysis and browning. In nature killer (NK) cells, *SNORD46* suppresses the IL15-dependent autophagy, leading to reduced viability of obese NK. *SNORD46* power inhibitors exhibit anti-obesity effects concurring with improved viability of obese NK, and anti-tumor immunity of CAR-NK cell therapy. Hence, our findings demonstrate the functional importance of snoRNAs in obesity and the utility of snoRNA power inhibitors for antagonizing obesity-associated immune resistance.

Keywords

Small Nucleolar RNA; Interleukin-15; Obesity; Adipocyte; Nature Killer cells; Lipase; Autophagy

Introduction

The global prevalence of obesity has increased dramatically both in adults and youth in the past few decades[1]. Obesity has been long considered one of the major risk factors for a myriad of chronic diseases, including type 2 diabetes, heart disease, and cancer[2]. Furthermore, diet-induced obesity accelerates tumor growth through impairing CD8^{+} T cell function in the tumor microenvironment (TME), indicating that obesity further impedes the immune checkpoint blockade-based treatment effects in cancer patients[3]. Current therapeutic options are limited in obesity and effective therapeutic opportunities are urgently needed to dampen the broad prevalence of obesity worldwide.

IL15 is well known as a stimulator of CD8^{+}T cells, natural killer (NK) cells and intraepithelial lymphocytes[4], while also acting as a circulating regulator of body composition[5]. IL15 acts as an anti-obesity cytokine by accelerating the lipid catabolism[5]. IL15 administration decreases white adipose tissue mass and lipoprotein lipase activity in *ob/ob* mouse without changing the food intake[6]. IL15 has shown extensive therapeutic prospects in maintaining lipid homeostasis, which is especially important for the treatment of obesity. However, the molecular mechanism underlying the anti-obesity effect of IL15 remains vague. The introduction of chimeric antigen receptor (CAR) to immune cells, including T-cells (CAR-T) and NK cells (CAR-NK), is under rapid development[7,8]. IL15 has been shown to stimulate NK cells in promoting an anti-tumor response in a variety of murine tumor models[9,10]. IL15 agonists or recombinant IL15 have been evaluated in clinical trials in combination with immune checkpoint blockers such as anti-PD-L1 antibodies[11]. The expression of IL15 significantly increased the cytotoxicity and persistence of NK cells *in vivo*[12]. However, obesity-dependent impairment of anti-tumor immunity has yet to be overcome.

Serum small nucleolar RNAs (snoRNAs) have raised attention as potential biomarkers for a variety cancer patients[13]. Here, we profiled snoRNA copies in obese serum, finding that Small Nucleolar RNA, C/D Box 46 (*SNORD46)* was increased in human donors with obesity. *SNORD46* copies correlate with BMI. Our findings suggested that saturated fatty acid triggered *SNORD46* expression in a phosphorylation of C/EBPβ (CCAAT/enhancer-binding protein beta)-dependent manner. The adipocyte-expressed *SNORD46* is directly associated with IL15 in serum, by which G11A mutant enhanced the affinity of *SNORD46*-IL15 interaction. We generated knockin mice harboring the G11→A mutation of *Snord46* (referred to as *Snord46*[G11A/G11A]). *Snord46*[G11A/G11A] mice exhibit obesity, reduced energy expenditure, impaired glucose metabolism, and liver steatosis. Mechanistically, ligand-bound IL15 receptor complexes triggered the phosphorylation of MGLL at Y268, resulting in augmented lipolysis activity; and CD36 at Y370, regulating the transportation of non-esterified fatty acids (NEFA, or free fatty acids, FFA), These events led to the accumulation of intracellular NEFA and adipocyte browning. The elevated *SNORD46* level or mutated *SNORD46* disrupted IL15-IL15 receptor complex, resulting in inhibited signaling events mentioned forehead and obesity. Further, excessive *SNORD46* inhibited the IL15-dependent autophagy in NK cells, leading to impaired antitumor immunity of NK cells under obesity condition. Administration of *SNORD46* power inhibitors antagonized the inhibitory role of *SNORD46 in vivo*, leading to the anti-obesity effect and sensitization of the breast and colorectal cancers to CAR-NK cells under obese conditions. Hence, our findings demonstrated the functional importance of snoRNAs in obesity and immune resistance.

Results

Serum *SNORD46* correlates with obese and immune suppressive tumor microenvironment

To study snoRNAs in obesity and cancer, we first utilized snoRNA array to determine snoRNA copies in human serum collected from donors with and without obesity, finding that *SNORD46* copies are increased in obese serum (Figures 1A, S1A–S1C; Table S1 and Data S1). We further validated *SNORD46* copies in human serum collected from 382 donors

with BMIs ranging from 16 to 78. The *SNORD46*, but not *U6* copies were significantly increased in the serum of BMI 30-40 group compared with BMI < 25 group, and further elevated in BMI > 40 group (Figure 1B). *SNORD46* copies correlated with BMI of donors with obesity (Figure S1D). We then examined *SNORD46* expression in human and mouse tissues, finding that adipose tissue exhibited the highest expression level of this snoRNA (Figure S1E). Northern blot confirmed the correlation between serum *SNORD46* level and BMI (Figure 1C). Furthermore, *SNORD46* expression was upregulated in omental (OM) and subcutaneous (SubQ) adipose, but not brown adipose tissue (BAT) tissue (Figures 1D and S1F). Serum *SNORD46* copies was reduced in donors with regular exercise (> 420 min/week) compared with donors without exercise (0 min/week) (Figure 1E). Consistently, serum *SNORD46*, but not *U6* copies negatively correlated with exercise time of donors with or without obesity (Figures 1F and S1G).

TCGA analysis indicated that tumors harbor elevated *SNORD46* level compared with adjacent normal tissues (Figure S1H). *SNORD46* level corelated with reduced tumor-resident infiltration of NK cells in colon cancer (COAD), breast cancer (BRCA), and other types of cancer (Figure 1G) and negatively correlated with immunophenotypic score (IPS) (Figure 1H). Tumors from breast cancer patients with high serum *SNORD46* copies exhibited reduced tumor-resident CD8^{+} T cells and NK cells (marked by NCAM1/CD56)[14], compared with those with low serum *SNORD46* copies (Figures 1I and 1J; Table S2).

Saturated fatty acid induces *SNORD46* expression *via* C/EBPβ

To determine the transcriptional factors that regulate *SNORD46* expression, we performed proteomics of isolated chromatin segments (PICh), finding a cohort of transcription factors associated with the promoter region of *SNORD46* (Figure 2A; Data S1). We then knocked down individual transcriptional factors in human adipocytes (HAd) validated by immunoblotting and RT-qPCR (Figures S2A and S2B), identifying that C/EBPβ is essential for *SNORD46* expression (Figure 2B). Mutagenesis studies confirmed that C/EBPβ T235A abolished *SNORD46* expression (Figures 2C and S2C), while C/EBPβ phospho-mimic mutants T235D or T235E, enhanced *SNORD46* level in the supernatant of C/EBPβ-deficient human adipocytes (Figure 2C). The recruitment of C/EBPβ to the promoter region of *SNORD46* was phospho-T235 dependent (Figure 2D). *Cebpb*-deficient mouse adipocytes (MAd) exhibited reduced *Snord46* expression, which was restored by C/EBPβ T188E mutant (Figures S2D–S2F). We challenged the high-fat diet (HFD)-induced obese mice with the treadmill exercise (TE), finding that HFD induced C/EBPβ T188 phosphorylation, which was reversed upon the TE (Figure 2E). Consistently, HFD-fed mice showed increased serum *SNORD46* copies, which was reduced by TE (Figures 2F and 2G). Interestingly, saturated fatty acids induced C/EBPβ (T235) phosphorylation, as well as supernatant *SNORD46* copies of human adipocytes (Figures 2H and 2I; Table S3).

SNORD46 is associates with IL15 and modulates IL15-dependent signaling

Liquid chromatography-mass spectrometry (LC-MS) analysis identified that biotinylated *SNORD46* was associated with IL15 (Figure 3A; Data S1), while biotinylated *miR20-a* was associated with AGO2, which is consistent with previous findings[15]. *SNORD46/Snord46*-IL15 interaction was validated by Cross-linking immunoprecipitation (CLIP) assay in

human and mouse serum respectively (Figures 3B and 3C). The *SNORD46*/*Snord46* motifs responsible for IL15 binding were also identified by CLIP assay (Figure 3C; Data S1). We next determined the single nucleotides of *SNORD46* responsible for IL15 binding in a rescue experiment using *SNORD46*-deficient adipocytes (Figures S3A–S3C), finding that mutation of G11C abolished *SNORD46*-IL15 interaction (Figure S3D), while G11A enhanced the *SNORD46*-IL15 interaction, and G11C/U impaired interaction with IL15 (Figure 3D).

We next performed limited proteolysis (LiP) followed by LC-MS analysis (LiP-MS)[16,17] to determine IL15 residues responsible for *SNORD46* binding. The LiP-MS analysis confirmed that the peptide recovery of N-termini of IL15 was increased in the presence of *SNORD46* RNA oligonucleotides, indicating that a.a. 1-8 of IL15 might be involved in interacting with *SNORD46* (Figure 3E; Data S1). Previous structural and mutagenesis studies have indicated that the D8 of IL15 plays important role in mediating IL15 receptor binding[18,19]. Our mutagenesis screening of IL15 a.a. 1-8 suggested that D8A mutation of IL15 impaired the *SNORD46* binding, while the D8S mutant enhanced *SNORD46* binding affinity (Figure 3F).

We further validated *SNORD46*-IL15 interaction by computational modeling using crystal structure of IL15 (PDB ID: 2Z3Q) for RNA-protein docking [20–22](Yan et al., 2017), finding that D8 and N65 of IL15 forms hydrogen bond with *SNORD46* G11, which stabilizes the *SNORD46*-IL15 complex (Figure 3G). The N1 of G11 forms a hydrogen bond with N65, then N65 directly interacts with D8 (Figure 3G). Interestingly, D8-N65 interaction is one of the only two polar interactions between the two alpha helixes (the other one is at the edge of the alpha helix), suggesting that this interaction is critical to maintain the conformation of IL15 to bind *SNORD46* (Figure 3G). With the mutation from guanine to adenine at nucleotide 11 of *SNORD46*, the carbonyl group was replaced with an amine group, which can form an additional hydrogen bond with N65 compared with guanine (Figure 3H). Thus, the binding affinity between *SNORD46* and IL15 is increased. With the mutation from aspartic acid to serine at ammino acid 8 of IL15, the carboxylic acid group was replaced with a hydroxyl group (Figure S3E). The hydroxyl group can be both a hydrogen bond acceptor and donor, while carboxylic acid can only accept hydrogens. The hydroxyl group may form a hydrogen bond with the backbone of *SNORD46*, while maintain the interaction with N65 (Figure S3E). Thus, the interaction between *SNORD46* and IL15 is increased. This computational modeling was validated in a RIP rescue experiment using IL15- or *SNORD46*-depleted human adipocytes with comparable levels of exogenously expressed WT or mutant of IL15 and *SNORD46* respectively (Figures 3I, 3J, and S3F–S3I).

IL15 has been suggested to reduce WAT mass in obese mice models[23]. However, the underlying molecular mechanism is largely unknown. We determined the gene expression profile of human adipocytes (BMI < 30) treated with vehicle or IL15 (**GSE210203**). Adipocytes isolated from healthy donors exhibited reduced expression of gene signatures related to Adipogenesis and Fatty Acid metabolism upon IL15 stimulation, which is consistent with the previous notion that IL15 exhibits an anti-obesity effect (Figure S3J). Taken together, our findings suggested that *SNORD46* physically interact with IL15 and acts

as a natural IL15 antagonist in the serum of donors with obesity to hinder the anti-obese effect of IL15.

SNORD46 G11A mutation drives obesity *in vivo*

Given that *SNORD46* is highly conserved between humans and mice, with 92.3% identity, we generated a knockin mouse model harboring a single-nucleotide variant (G11→A) of the mouse *Snord46* gene using CRISPR/Cas9-mediated technology (Figure 4A). Male and female homozygous mice harboring the AA mutant (*Snord46*[G11A/G11A]) exhibited augmented body weight compared with WT or heterozygous littermates (Figures 4B and 4C). Body composition analysis indicated that *Snord46*[G11A/G11A] mice exhibited increased body weight, fat weight, and fat percentage (Figures 4D–4H). Histological analysis indicated that *SNORD46*[G11A/G11A] mice exhibited increased adipose tissue, enlarged islet areas, and liver steatosis (Figures 4I and 4J). Comprehensive Lab Animal Monitor System (CLAMP) analysis indicated that *Snord46*[G11A/G11A] mice exhibited reduced oxygen consumption (VO2), reduced carbon dioxide production (VCO2), and reduced energy expenditure (Figures 4K, 4L, and S4A–S4D). Female *Snord46*[G11A/G11A] mice exhibited increased food intake whereas male *Snord46*[G11A/G11A] mice showed unaltered food intake compared with *Snord46*[WT/WT] mice (Figure S4E). Male *Snord46*[G11A/G11A] mice showed increased water intake in compared with *Snord46*[WT/WT] littermates (Figure S4F). Further, *Snord46*[G11A/G11A] mice exhibited significantly impaired glucose tolerance (Figures 4M and S4G). Compared with WT littermates, *Snord46*[G11A/G11A] mice exhibited reduced body temperature, increased urine volume, blood triglycerides, AST, and ALT concentrations (Figures S4H–S4L). Both male and female *Snord46*[G11A/G11A] mice had similar serum leptin level[24] compared with WT mice (Figure S4M). The serum Ghrelin[24,25] level is unaffected in *Snord46*[G11A/G11A] mice compared with WT mice (Figure S4N). Furthermore, both male and female *Snord46*[G11A/G11A] mice showed increased serum insulin level compared with *Snord46*[WT/WT] mice (Figure S4O). Hence, our findings suggested that *SNORD46* contributes to the obesity, which is independent on its neighboring gene *RPS8* (Figures S5A–S5D).

IL15 triggers a non-canonical signaling cascades in adipocytes

We aimed to compare the signaling pathways of IL15 in the major organs between *Snord46*[WT/WT] and *Snord46*[G11A/G11A] mice by identifying IL15-binding proteins. Interestingly, IL15 was associated with IL15Rα and tyrosine-protein kinase JAK3 in brain, heart, liver, skeletal muscle (SKM), spleen, and intestine of *Snord46*[WT/WT] mice, which are components of the conventional IL15 signaling pathway[11] (Figure 5A; Data S1). In WAT, IL15 was associated with tyrosine-protein kinase FER, Monoglyceride Lipase (MGLL), and Platelet glycoprotein 4 (CD36), triggering a potentially unconventional pathway (Figure 5A). The association between IL15 and conventional/unconventional signaling pathway components were diminished in *SNORD46*[G11A/G11A] mice (Figure 5A). The MS also revealed that FER was phosphorylated at Y402; MGLL was phosphorylated at Y268; and CD36 was phosphorylated at Y370 (Figures S5E–S5G). We generated modification specific antibodies targeting human p-MGLL Y268, or p-CD36 Y370, which were validated using peptide-blocking assays (Figures S5H and S5I). Hence, we reason that upon ligand binding, IL15 receptor complex recruits FER, which mediates the downstream signaling cascades.

We verified the interactions between mouse IL15 and IL2Rβ, MGLL, and CD36, which were enhanced by IL15 but abolished by *SNORD46* G11A mutant in mouse adipocytes (Figure 5B).

To examine whether *SNORD46* mutant modulates IL15-IL2Rβ interaction, we performed *in vitro* pulld-own assay using His-tagged IL15 (Figure 5C). IL15 exhibited adequate interactions with IL2Rβ; in the presence of *SNORD46*, IL15 WT exhibited reduced interaction with IL2Rβ, which were further abolished in the presence of *SNORD46* G11A mutant (Figure 5C). The presence of *miR-20a* showed minimal effect on the IL15-IL2Rβ interaction (Figure 5C). *SNORD46* G11C or G11U mutants exhibited a minimal effect on the interaction between IL15 and IL2Rβ (Figure 5C). Our findings suggested that *SNORD46* inhibited the interaction between IL15 and the receptor complex. *SNORD46* G11A showed a robust inhibitory effect on the IL15 ligand-receptor binding.

To further characterize IL15-triggered, FER/MGLL/CD36-medicated unconventional pathways in adipocytes, we determined that in adipocytes, IL15 induced the p-FER (Y402), p-MGLL (Y268), p-CD36 (Y370), but not in NK cells (Figure 5D). The IL15 induced-p-FER (Y402), -p-MGLL (Y268), and -p-CD36 (Y370) were abolished by *Il2rb* depletion or *Snord46* G11A mutation (Figure 5E). IL15 also upregulated the protein level of mitochondrial brown fat uncoupling protein 1 (UCP1), PR/SET domain 16 (PRDM16), cell death inducing DFFA like effector A (CIDE-A), and peroxisome proliferator-activated receptor gamma (PPARγ) (Figure 5F), which are essential factors of WAT browning[26]. The UCP1, PRDM16, CIDEA, or PPARγ levels were reduced by *IL2Rb* depletion, or *SNORD46* G11A mutation (Figure 5F). The reduced UCP1 and PPARγ levels were verified in *Snord46*[G11A/G11A] WAT compared with *Snord46*[WT/WT] WAT (Figures S5J and S5K).

The obesity phenotype of *Snord46*[G11A/G11A] mice inspired us to further validate the concentrations of intracellular/ extracellular non-esterified fatty acids (NEFA) and intracellular triacylglycerol (TG). Our data showed that IL15 triggered reduction of intracellular TG with concurrent increased intracellular NEFA and decreased extracellular NEFA (Figures 5G–5I). *Il2rb* deficiency or *Snord46* G11A mutation in adipocytes abolished IL15's effect, resulting in elevated intracellular TG, reduced intracellular NEFA, as well as increased extracellular NEFA (Figures 5G–5I). The intracellular NEFA stimulates FA oxidation and oxygen consumption of adipocytes[27]. We hence determined the oxygen consumption rate (OCR) of mouse adipocytes isolated from *Il2rb* KO or *Snord46*[G11A/G11A] mice, finding that IL15 triggered the oxygen consumption of adipocytes and *Il2rb* depletion, or *Snord46* G11A mutation reduced OCR compared with the adipocytes isolated from WT mice (Figure 5J). Taken together, our findings suggested that IL15 inhibits obesity *via* an unconventional signaling cascade promoting lipolysis of adipocytes, which can be antagonized by *SNORD46*.

Phosphorylation of MGLL and CD36 modulates lipolysis and FA transportation

MGLL converts monoacylglycerides to free FA and glycerol and is an essential enzyme in the lipolysis[28]. Hence, we measured the glycerol production catalyzed by recombinant MGLL, finding that the phosphorylated MGLL, or phospho-mimic mutant Y268E (YE) exhibited increased enzymatic activity compared with unphosphorylated MGLL (Figure

S5L). In human adipocytes, IL15 led to enhanced glycerol production, in which the enzymatic activity of MGLL was abolished upon MGLL depletion (Figure S6A). The expression of exogenous MGLL WT, but not YF mutant, rescued the glycerol production in MGLL-deficient cells (Figure S6A). Furthermore, the phospho-mimic mutant YE, but not YD restored enzymatic activities of MGLL (Figure S6A). Consistently, adipocytes with MGLL KO exhibited increased intracellular TG with concurrent reduced intracellular NEFA (Figures 5K and 5L). Expression of MGLL WT restored IL15-induced NEFA catalysis (Figures 5K and 5L). Furthermore, adipocytes with MGLL YE mutant exhibited decreased TG and enhanced NEFA concentration (Figures 5K and 5L). Consequently, adipocytes with MGLL KO exhibited abolished expression of UCP1, PRDM16, CIDEA, and PPARγ, which was restored upon the expression of MGLL WT or YE mutant (Figure S6B). In addition, MGLL WT or YE mutant rescued the OCR of *MGLL*-deficient adipocytes (Figure S6C).

CD36 is a fatty acid translocase, playing important roles in binding with long chain fatty acids (LCFA) and transportation of LCFAs into cells[29]. Our findings suggested that CD36-proficient adipocytes exhibited normal FA uptake, which was inhibited by IL15 (Figure S6D). Knockout of CD36 abolished the FA uptake, which was restored by WT CD36 (Figure S6D). The CD36 Y370F (YF) mutant enhanced FA uptake; Y370D (YD) or Y370E (YE) phospho-mimic mutants further reduced FA uptake (Figure S6D). Our findings suggested that the CD36-dependent FA uptake is regulated by the IL15-triggered phosphorylation of CD36 at Y370. It is interesting to observe that the extracellular NEFA concentration of adipocytes was reduced by IL15 (Figure S6E). CD36 depletion resulted in elevated extracellular NEFA, which was restored by exogenous CD36 WT or YD mutant (Figure S6E).

We further strengthen the molecular linkage of *SNORD46* to IL15-dependent FER/CD36/ MGLL signaling cascade in *Il2rb*-deficient adipocytes rescued with FER YD, MGLL YE, CD36 YD, or MGLL YE + CD36 YE mutants (Figure S6F). It is noteworthy that FER phospho-mimic mutants (Y420D, YD) restored UCP1, PRDM16, CIDEA, and PPARγ protein levels in *Il2rb*-deficient adipocytes (Figure S6F). MGLL YE or CD36 YD mutant alone exhibited partial rescue on UCP1, PRDM16, CIDEA, and PPARγ protein levels in *Il2rb*-deficient adipocytes, however, MGLL YE + CD36 YE mutants robustly rescued the levels of these proteins in *Il2rb*-deficient adipocytes (Figure S6F). Consistently, *Il2rb*-deficient adipocytes exhibited elevated intracellular TG and extracellular NEFA concentrations, with concurrent reduced intracellular NEFA concentration, which were restored by FER YD mutant independent on IL15 treatment (Figures S6G–S6I). CD36 YD mutant alone failed to rescue the IL15-induced intracellular TG hydrolysis and concurrent NEFA export in *Il2rb*-deficient adipocytes (Figures S6G and S6I). However, *Il2rb*-deficient adipocytes with MGLL YE or MGLL YE + CD36 YE mutants exhibited the restored intracellular TG hydrolysis and concurrent NEFA export (Figures S6G and S6I). Consistent with this notion, MGLL YE or MGLL YE + CD36 YE mutants rescue the OCR of *Il2rb*-deficient adipocytes (Figure S6J). Taken together, our findings demonstrated that IL15 triggers an unconventional FER/CD36/MGLL-medicated signaling cascades in adipocyte to modulate the cellular FA transportation and lipolysis.

SNORD46 inhibitors antagonize obesity

We next screened *SNORD46* power inhibitors that can abolish *in vivo SNORD46*-IL15 interaction by MS (Figure 6A**; Table S10**). *SNORD46* power inhibitor #4 (referred to as *SNORD46* pi) specifically abolished the IL15 protein binding using biotinylated *SNORD46* as a bait (Figure 6A; Data S1). In serum of donors with obesity, the specific inhibitory effect of *SNORD46* pi and IL15 neutralizing antibody (NAb) on suppressing *SNORD46*-IL15 interaction was verified by northern blotting and immunoblotting (Figures 6B and S7A–S7C). We further determined the effect of *SNORD46* pi on *SNORD46*-IL15 interaction in human serum (Figure 6C), finding that the presence of *SNORD46* pi abolished the interaction between IL15 and *SNORD46* G11A mutant with minimal effect on *miR-20a*-AGO2 interaction (Figure 6C).

Compared with adipocytes of BMI < 30 group, BMI > 40 adipocytes exhibited reduced level of p-FER (Y420), p-MGLL (Y268), and p-CD36 (Y370), in the absence of IL15 (Figure 6D, lane 9 *vs.* lane 1). For BMI < 30 adipocytes, IL15 induced p-FER (Y420), p-MGLL (Y268), and p-CD36 (Y370) respectively (Figure 6D, lane 2 *vs.* lane 1). However, for BMI > 40 adipocytes, IL15 showed undetected effect on p-FER (Y420), p-MGLL (Y268) and p-CD36 (Y370) (Figure 6D, lane 10 *vs.* lane 9). *SNORD46* pi sensitized BMI < 30 adipocytes to IL15 stimulation, leading to the enhanced p-FER (Y420), p-MGLL (Y268), p-CD36 (Y370) and UCP1, PRDM16, CIDEA and PPARγ protein levels (Figure 6D, lane 4 *vs.* lane 3). Furthermore, for BMI > 40 adipocytes, *SNORD46* pi facilitated the IL15-induced p-FER (Y420), p-MGLL (Y268) and p-CD36 (Y370) respectively, as well as the protein levels of UCP1, PRDM16, CIDEA and PPARα (Figure 6D, lane 12 *vs.* lane 11).

We next measured the intracellular TG, NEFA and extracellular NEFA concentration of BMI < 30, 30-40, or > 40 adipocytes, finding that IL15 induced reduced intracellular TG, extracellular NEFA with elevated intracellular NEFA concentration of BMI < 30 adipocytes (Figures 6E, 6F, and S7D). However, IL15 showed minimal effect on these for BMI > 40 adipocytes (Figures 6E, 6F, and S7D). *SNORD46* pi sensitized BMI > 40 adipocytes to IL15, leading to reduced intracellular TG, elevated intracellular NEFA and decreased extracellular NEFA concentration (Figures 6E, 6F, and S7D). Consistently, BMI > 40 adipocytes exhibited reduced OCR compared with BMI < 30 adipocytes, which can be restored by which *SNORD46* pi (Figure S7E).

Furthermore, *Snord46* pi decreased the body weight and improved the glucose tolerance of *Snord46*^G11A/G11A mice significantly compared with scramble sequence, Orlistat and Liraglutide (two FDA-approved anti-obesity drugs) (Figures 6G, S7F, and S7G). *Snord46* pi treated *Snord46*^G11A/G11A mice exhibited reduced liver steatosis, fatty acid accumulation, and increased protein levels of UCP1 and PPARγ in WAT (Figures 6H and S7H). The HFD-fed mice receiving *Snord46* pi treatment also displayed a significant decrease in lipid accumulation in the liver (Figure S7I). Hence, our findings suggested that inhibition of *SNORD46* may block *SNORD46*-IL15 interaction and antagonize obesity *in vivo*.

Targeting *SNORD46* restores anti-tumor immune microenvironment

NK cells in obese patients have been indicated to exhibit reduced cytotoxic capabilities[30,31]. Hence, we next tested whether the elevated *SNORD46* contribute to the reduced cytotoxicity of obese NK cells using NK cells isolated from PBMCs of healthy donors with BMI < 25 (referred to as normal NK) and donors with obesity (BMI > 35) (referred to as obese NK) (Table S4). We first noticed that NK cell number was reduced in donors with obesity compared with normal donors, which was consistent with previous findings[30] (Figures S8A and S8B). Similarly, NK cell number was reduced in peripheral blood of *Snord46*$^{G11A/G11A}$ mice compared with *Snord46*$^{WT/WT}$ littermates (Figure S8C). Transcription profiling indicated that obese NK cells with high *SNORD46* expression exhibited reduced inflammatory response, TNFα signaling, and JAK/STAT3 signaling, which is independent on *SNORD46*'s neighboring gene *RPS8* (Figures 7A and S8D–S8G; **GSE213465**). Obese NK cells also showed reduced autophagy gene signature (Figure 7B; Data S1), suggesting impaired autophagy response. We validated the reduced expression of LC3A/B in NK cells isolated from BMI > 35 group, compared with normal BMI group (Figure 7C). Consistently, obese human NK cells or mouse *Snord46*$^{G11A/G11A}$ NK cells showed impaired cell viability in the presence of an autophagy inducer, Tubeimoside I (TBM)[32] (Figures 7D and 7E). *SNORD46* pi significantly enhanced the cell viability of NK cells isolated from donors with obesity or *Snord46*$^{G11A/G11A}$ mice (Figures 7F and 7G).

To test whether *SNORD46* pi augments the cytotoxicity of obesity-associated NK cells and sensitizes tumors to CAR-NK cell therapy under the obese condition, we generated two CAR-iPS cells engineered to express either EGFR-CAR[33,34] or CD133-CAR[35,36] and were subsequently differentiated into NK cells with high specificity and purity (Figures S8H and S8I). EGFR-CAR-iPS-NK exhibited anti-tumor immunity against the human triple-negative breast cancer (TNBC) cells (MDA-MB-231), while CD133-CAR-iPS-NK cells showed cytotoxicity to the human colorectal adenocarcinoma cells (HT-29) (Figures S8J–S8L). HT-29 tumor growth was significantly inhibited by CD133-CAR-iPS-NK cells under chow condition (Figure 7H, left). However, under the condition of HFD-induced obesity, administration of CD133-CAR-iPS-NK cells showed a marginal effect on the growth of the HT-29 tumor (Figure 7H, right). *SNORD46* pi significantly improved the anti-tumor immunity of these CAR-NK cells (Figure 7H). Similarly, EGFR-CAR-iPS-NK cells significantly inhibited the growth of the MDA-MB-231 tumor under the chow-fed condition, but not under HFD-induced obesity (Figure 7I). Animals subjected to *SNORD46* pi treatment exhibited reduced MDA-MB-231 tumor burden upon EGFR-CAR-iPS-NK administration under both chow and HFD-fed conditions (Figure 7I). We next determined the status of CAR-iPS-NK cells in tumors of normal or obese mice, finding that both MDA-MB-231 and HT-29 xenograft harbored reduced NK cells upon HFD challenge, which were restored by *SNORD46* pi (Figures 7J and 7K). Taken together, these data suggested a precisely targeted combinatorial treatment for obesity and obesity-associated immune resistance through the application of a snoRNA-based approach.

Discussion

Human subject studies suggested that plasma IL15 concentration negatively correlates with BMI, and fat mass[37,38]. Mice with *Il15* knockout (*Il15*−/−) results in significant increase in weight gain without altering appetite[5,23]. Transgenic mice with elevated circulating IL15 exhibited reduced weight of body fat and resistant to diet-induced obesity[39]. Introduction of recombinant IL15 by protein injection[40], adenoviral expression vector[5] or DNA electrotransfer[37], all resulted in reduced fat mass in rodents, but no effect on food intake nor lean body mass. Our research work suggests that *SNORD46* inhibits the normal biology of IL15 in lipid metabolism, leading to inhibited lipolysis and adipose browning, which is unlikely indirect effect on modified energy intake. The exact role of IL15 and *SNORD46* signaling axis in obesity warrants the future investigation using tissue specific *Il15/Snord46* knockout mice.

MGLL plays an important role in converting monoacylglycerides to FFA and glycerol, which is the rate-limiting step of lipolysis[41]. *Mgll* knockout mice exhibit resistance to obesity induced by HFD[42]. Histidine-269 plays an essential role in the catalytic triad of MGLL, forming a hydrogen bond with substrate[43]. Hence, it is possible that the phosphorylation of Y268 identified by our studies may affect the release of substrate and lead to altered enzymatic activity of MGLL. Genetic evidence indicated that *Cd36*-deficient mice exhibited significant decrease in binding and uptake of oxidized low-density lipoprotein[44], signifying the essential role of CD36 in lipid transportation. Our findings suggested the FER-mediated phosphorylation of CD36 inhibits FA uptake. We reason that the phosphorylation of CD36 is likely to modulate the cycling of CD36. The roles of other lipase, including ATGL, HSL, and lipid transporters in IL15 induced lipolysis warrants further investigation.

Overall, our studies demonstrated the underlying mechanism of obesity in an IL15 and *SNORD46*-dependent manner. In this study, we focus on targeting *SNORD46* by pi as a promising therapeutic strategy for alleviating obesity and augmenting the anti-tumor immunity of CAR-NK cells. Thus, in the future, it is worthwhile to study the snoRNAs as the primary interplaying factors that constitute metabolism, immunological reactions, and cancer with a focus on mechanistic aspects. Finally, our studies reveal the possibility of metabolic interventions at non-coding RNA level to enhance the efficacy of immunotherapeutic and conventional approaches for future anti-obesity and -cancer treatments.

Limitations of the study

In *in vitro* biochemical studies, we identified that *SNORD46*-IL15 interaction is significantly enhanced by *SNORD46* G11A mutation. Although genetic knockin *SNORD46* G11A mutation drives the obesity and spontaneous tumor development in multiple organs of mice, it is not clear if this mutation affects IL15 signaling to regulate obesity or contribute to NK cell pathophysiology and cancer development in human. Technically, since most experiments were conducted with mouse and human adipocytes, we appreciate its intraindividual variability, and genome editing in these adipocytes did not reach complete KO. Moreover, we cannot fully exclude putative off-target effects of the *SNORD46* inhibitor

used. Our *Snord46*$^{WT/G11A}$ mice did not show any phenotypes. It is possible that the expression of the knockin allele does not follow a simple gene dosage effect. The wild-type allele may compensate for the effects of the knockin allele, preventing the obese phenotype from manifesting. This compensation could occur at the transcriptional, translational, or post-translational levels.

STAR★Methods

Resource Availability

Lead contact—Further information and requests for resources and reagents should be directed to and will be fulfilled by the lead contact, Liuqing Yang (lyang7@mdanderson.org).

Materials availability—All unique/stable reagents generated in this study are available from the lead contact under Material Transfer Agreement.

Data and code availability

- The bulk RNA-seq of human adipocytes with or without IL15 stimulation were deposited to GEO (**GSE210203**). The bulk RNA-seq of NK cells isolated from healthy donors and donors with obesity were deposited to GEO (**GSE213465**).

- **Data S1**: Unprocessed source data underlying all blots and graphs, related to Figures 1, 2, 3, 4, 5, 6, 7, and S1–S8. This file includes: 1) Uncropped hi-resolution scans of all the blots; 2) Excel file containing the values that were used to create all graphs in the paper; 3) Normalized expression value of snoRNA PCR array; 4) Protein identification data of PICh-MS; 5) Protein identification data of *SNORD46*-binding proteins; 6) Sanger sequencing results of IL15 CLIP assays; 7) Peptide identification data of IL15 LiP-MS assay; 8) Protein identification data of IL15 binding proteins in the major organs of *Snord46*$^{WT/WT}$ or *Snord46*$^{G11A/G11A}$ mice; 9) Mass spectrometry verification data of *SNORD46* power inhibitors; 10) Normalized expression value of bulk-RNA seq in NK cells.

- This paper does not report original code.

- Any additional information required to reanalyze the data reported in this paper is available from the lead contact upon request.

Experimental model and subject details

Study approval—Human tissue studies were deemed exempt by the Institutional Review Board (IRB) of MD Anderson Cancer Center due to the fact that only de-identified human samples were utilized, while the human induced pluripotent stem (hiPS) cell studies are approved by HEIP Stem Cell committee of MD Anderson Cancer Center. All animal studies were approved by the Institutional Animal Care and Use Committee (IACUC) of MD Anderson Cancer Center.

Tissue, serum, and primary cells—Human serum samples from donors with BMI and clinical parameters were purchased from the following commercial vendors: Asterand Bioscience, BioIVT, Proteogenex, Reprocell USA and Coriell Biorepository (Table S1). Human breast cancer tumor tissues and paired serum samples with clinical information were obtained from Discovery Life Sciences. Clinical information is listed in Table S2. Primary human pre-adipocytes were purchased from Zen-Bio, Cell Applications and Celprogen. BMI and clinical parameters are listed in Table S3. Human PBMC from healthy donors or donors with obesity were obtained from STEMCELL Technologies. BMI and clinical parameters are listed in Table S4. Human and mouse tissue total RNA were purchased from Zyagen.

Mouse models and *in vivo* treatment—By using CRISPR/Cas9 Extreme Genome Editing System (EGE™ Biocytogen), we knocked in a one-nucleotide mutant to mouse *SNORD46* gene Chr4:117,155,277 C>T in C57BL/6N mice to achieve the mouse *Snord46* G11A mutant, which is the residue conserved in human *SNORD46* G11A. C57BL/6, *Cebpb*$^{-/-}$ mice, *Il2rb*$^{-/-}$ mice used in this study were purchased from The Jackson Laboratory. To establish the high fat diet (HFD) animal model, mice were fed with HFD (Research Diets) starting at 6-weeks age. To obtain unbiased and reliable results, mice were randomly grouped for all experiments and at least five mice were used in each group. For pi treatment, *Snord46*$^{WT/WT}$ and *Snord46*$^{G11A/G11A}$ mice were treated with *Snord46* pi (1 mg/kg, subQ, every 3 days). For the treatment of Orlistat or Liraglutide, *Snord46*$^{G11A/G11A}$ mice were treated with orlistat by oral (10 mg/kg/day)[45] or Liraglutide *via* subQ delivering (0.4 mg/kg/day)[46]. To identify the IL15 binding proteins in WAT, biotinylated IL15 were injected to the *Snord46*$^{WT/WT}$ or *Snord46*$^{G11A/G11A}$ mice (10 mg/kg, ip. Once). 24-h post injection, major organs were collected, homogenized for streptavidin pull-down followed by mass spectrometry, which is described below. All animals were housed under a 12-h light/12-h dark cycle in the animal facility with free access to water and food. Sample size was indicated in each figure.

Pluripotent Stem Cells—The hiPS cell lines derived from skin fibroblasts of healthy donor were obtained from Human Stem Cell Core (HSCC) (Baylor College of Medicine) and cultured individually on hESC-Qualified Matrigel (Corning) coated plates and maintained in mTeSR™ plus medium (STEMCELL Technologies).

Method details

Plasmid, siRNAs, transfection, lentiviruses production and transduction—*SNORD46* and *SNORD46* DNA sequence was synthesized by GenScript and cloned into pGEM-3Z vector (Promega) for *in vitro* transcription and into the pcDNA3.1 (+) vector (Life technologies) for mammalian expression. Mammalian expression vector for C/EBPβ, IL15, *SNORD46* and corresponding mutants were constructed by VectorBuilder and packed in lentivirus. IL15, MGLL wild-type, and mutant sequences were synthesized and cloned into pET-28a (+) (GeneScript). The recombinant protein was expressed in *E. coli* strain BL21-CodonPlus (DE3)-RIPL (Agilent Technologies) and purified using HisPur™ Cobalt Purification Kit (Thermo Scientific). ON-TARGETplus siRNAs SMARTpool (Dharmacon™) used in this study were transfected using SilenceMag siRNA Delivery Reagent based on the Magnetofection™ technology (OZ Biosciences). Lentiviruses were

produced using pPACKH1 HIV Lentivector Packaging Kit (System Biosciences). Lentiviral transduction of sgRNAs and expression constructs were conducted using ViroMag CRISPR (OZ Biosciences) and ViroMag Stem Transduction Enhancer respectively.

Human snoRNA PCR array—The total RNA from serum of 6 healthy donors (BMI < 25) and 6 donors with morbid obesity (BMI > 40) were purified with the miRNeasy Serum/Plasma Kit (Qiagen) followed by cDNA synthesis using rtStar™ tRNA Pretreatment & First-Strand cDNA Synthesis Kit (ArrayStar). SnoRNA expression analysis was performed using nrStar™ Human snoRNA PCR Array (ArrayStar), which analyzed 359 H/ACA and C/D box snoRNAs. HK (Housekeeping genes; Internal Controls): 8 human housekeeping genes *ACTB*, *B2M*, *Gusb*, *Hsp90ab1*, *GAPDH*, *5S rRNA*, *28S rRNA*, and *18S rRNA* were included as the internal qPCR normalization references.

Human adipocyte culture and treatment—Human preadipocytes were obtained from various vendors and were cultured with DMEM/F12 medium with 5% fetal calf serum (added penicillin/streptomycin) at 37°C at 5% CO2. Adipogenic conversion was then promoted for 14 days by changing medium to DMEM/F12 without serum addition (penicillin/streptomycin), supplemented with 66 nM insulin, 100 nM dexamethasone, 0.5 mM IBMX, 0.1 mg/ml pioglitazone, 1 nM triiodo-L-thyronine, and 10 mg/ml human transferrin. After 5 days of incubation, medium was used as described before but without IBMX and pioglitazone for 9 more days[47]. Gene knockdown was performed to the preadipocytes by introducing siRNA and were further induced into mature adipocytes after confirming the expression level of individual genes. Gene targets were knocked out using the CRISPR/Cas9 genome editing system (VectorBuilder) followed by expressing the individual indicated expression constructs in preadipocytes. For supplementation assays, 5 days after the start of the induction process, the indicated unsaturated and saturated fatty acid were added directly to the cell culture well at each medium change. Treatment of adipocytes with fatty acids (Nu-Chek-Prep) were performed as previously described[48,49].

DNA and RNA isolation, quantitative real-time PCR—snoRNA was extracted from the human/mouse serum and adipocyte supernatant using miRNeasy Serum/Plasma Kit (Qiagen). Total RNA or snoRNA was isolated from human/mouse adipose tissue and adipocytes using RNeasy Lipid Tissue Mini Kit (Qiagen). For snoRNA detection, 1 μl of miRNeasy Serum/Plasma Spike-In Control (Qiagen) was added before RNA extraction as the reference gene for the following quantitative experiments. The *cel-miR39-3p* RNA spike-in template was used in combination with the *UniSp6* RNA spike-in template provided with the miRCURY LNA RT Kit (Qiagen) as the cDNA synthesis control. Quantitative real-time PCR was performed using the miRCURY LNA SYBR Green PCR Kit (Qiagen). For mRNA detection, reverse transcription and real-time PCR were performed using iScript™ cDNA Synthesis Kit and SsoAdvanced Universal SYBR Green Supermix (Bio-Rad). The RNA copy number was performed as previously described[50]. Briefly, the total RNA of the serum, adipocyte supernatant, and adipocyte samples were extracted and detected by qRT-PCR. A standard curve was generated by a serial dilution of *in vitro* transcribed *SNORD46* RNA, using 728908.2 for human *SNORD46* and 710082.8 for mouse *Gm26330*

as the molecular weight, and the total RNA per cell was estimated to be 20 pg. The primers used in these studies are listed in Table S5.

Northern blot—The RNA samples were separated by polyacrylamide gel electrophoresis with 6 M urea as a denaturing agent. The separated RNA sequences were transferred to the nylon membrane and subjected to blotting using NorthernMax® Kit (Thermo Fisher Scientific). The *in vitro*-produced biotinylated probes targeting *SNORD46/Snord46* or the control RNA were hybridized with RNA sequences on the nylon membrane, separately. After removing the non-hybridized probe, the blot membrane was then subjected to avidin attached to HRP (horseradish peroxidase). The labeled probe was detected by chemiluminescence to evaluate the molecular weight and the abundance of the RNAs in each sample.

Proteomics of isolated chromatin segments (PICh)—PICh was carried out as previously described[51] using the following 2'Fluoro-RNA probes for hybridization: Destiobiotin-108 atom tether- AaCgCaCaAcTgTcAcAcGgAa (*SNORD46* probe); Destiobiotin-108 atom tether-TtAgGgTtAgGgTtAgGgTtAgGgt (Telomere probe); Destiobiotin-108 atom tether-GaTgTgTgGaTgTggAtGtGgAtgTgg (Scramble probe).

Chromatin immunoprecipitation (ChIP)—Chromatin was prepared from human adipocytes after cross-linking for 10 min at room temperature with 1% formaldehyde-containing medium, using truChIP™ Chromatin Shearing Kit with Formaldehyde (Covaris). Nuclear extracts were sonicated using M220 Focused-ultrasonicator (Covaris) to obtain DNA fragments averaging 200 bp in length followed by immunoprecipitation overnight with 10 μg of C/EBPβ antibody (Table S6). Immunoprecipitation was washed in RIPA buffer [50 mM HEPES-KOH (pH 8), 500 mM LiCl, 1 mM EDTA (pH 8), 1% NP-40, 0.7% sodium deoxycholate followed by a TE/50 mM NaCl wash. Elution was performed at 65°C for 15 min with elution buffer [50 mM Tris-HCl (pH 8), 10 mM EDTA (pH 8), 1% SDS] and reverse crosslinked at 65°C overnight together with input. DNA was recovered by ChIP DNA Clean & Concentrator (Zymo Research). RT-qPCR was performed using SYBR green and CFX96 Real-Time PCR System (Bio-Rad) with primers listed in Table S5.

***In vitro* pull-down, immunoprecipitation, and immunoblotting**—For *in vitro* protein-protein interaction studies, the recombinant His-tagged full length IL15, and its mutants were incubated with biotinylated *SNORD46* or the control molecule at 4 °C for 16 h, and the Ni-NTA pull-down was performed in the presence of IL2RB using Pierce™ His Protein Interaction Pull-Down Kit (Thermo Fisher Scientific). The pull-downs were resolved by SDS–PAGE and analyzed by immunoblotting with the appropriate antibodies. The immunoprecipitation was performed using Dynabeads™ Co-Immunoprecipitation Kit (Thermo Fisher Scientific). The immunoprecipitates were separated by SDS–PAGE and immunoblotted with listed antibodies (Table S6). Visualization of the immunoblots was performed by Clarity Western ECL Substrate (Bio-Rad) according to the manufacturer's instructions.

RNA pull-down and mass spectrometry analysis—To identify *SNORD46*-binding proteins in serum, *SNORD46* pull-down was performed as previously described[17,52].

Briefly, biotin-labeled *SNORD46* RNAs were *in vitro* transcribed with Biotin RNA Labeling Mix (Millipore Sigma) and MEGAscript® Transcription Kit (Thermo Fisher Scientific), further purified by RNA Clean & Concentrator-5 (Zymo Research). Human serum proteins were purified using Aurum Serum Protein Mini Kit (Bio-Rad). The BcMag™ Monomer avidin Magnetic Beads (Bioclone) were prepared according to the manufacturer's instructions and then immediately subjected to RNA (20 μg) capture in RNA capture buffer [20 mM Tris-HCl (pH 7.5), 1M NaCl, 1mM EDTA] as previously described[52]. The eluted RNA-protein complexes were denatured, reduced, alkylated, and digested with immobilized trypsin (Promega) for mass spectrometry analysis at MD Anderson Cancer Center Proteomics Facility.

UV-Crosslinking and Immunoprecipitation (CLIP) assay and RIP assay—Human serum was UV crosslinked on ice with three irradiations of 254 nm UV-light at 400 mJ/cm2 in a UV crosslinker (Agilent). CLIP was performed using the IL15 antibody (Table S6) as previously described[53]. RNA-protein complexes of interest were then partially purified by immunoprecipitation, and non-covalently associated RNAs were removed by sodium dodecyl sulfate polyacrylamide gel electrophoresis (SDS-PAGE). RNA-protein complexes were subjected to SDS-PAGE and autoradiography. The RNA fragments were extracted, ligated, reverse transcribed, and ligated into the vector pCR-Blunt for Sanger sequencing. RIP assay was performed using Magna RIP™ RNA-Binding Protein Immunoprecipitation Kit (Millipore). Human serum was immunoprecipitated using 2.5 μg of normal rabbit IgG, anti-IL15 antibody or anti-Argonaute-2 antibody (Table S6). Immunoprecipitation of IL15-target and non-target associated RNA was validated by quantitative PCR (qPCR). CFX Manager software v.3.1 (Bio-Rad) was used for data acquisition for qPCR.

Determination of K_d value using Alpha assay—Alpha binding assays were used to quantitatively assess the interaction between *SNORD46* and IL15 using biotinylated *SNORD46* and His-tagged IL15 as the donor and acceptor pair[17]. The dissociation constant (K_d) was determined via a competition experiment in which WT *SNORD46*, or IL15 and their mutants were titrated (two-fold dilution) from 100 μM to 1 pM, separately. Streptavidin donor beads and anti-His6 AlphaLISA acceptor beads were used in these assays (PerkinElmer). The plates were read on the EnSpire Multimode plate reader (PerkinElmer). The competitive inhibition curves were calculated based on alpha signal readings by fitting to a log (inhibitor) versus response-variable slope (four parameters) model (GraphPad Prism 9).

Limited proteolysis (LiP)-coupled liquid chromatography–mass spectrometry (LC-MS)—LiP followed by LC-MS was adapted from LiP-SRM analysis[16]. Briefly, bacterially expressed IL15 (2 mg/ml) alone, in the presence of Scramble RNA or *SNORD46* RNA (2 mM) were incubated in buffer (20 mM HEPES, pH7.5, 150 mM KCl and 10 mM $MgCl_2$) and Protease K at room temperature for 5 min as limited proteolysis. The digestion was stopped by transferring the reaction mixture to a tube containing guanidine hydrochloride crystals to a final concentration of 7.4 M and by boiling for 3 min. The digestion mixtures were then subjected to complete Staphylococcal peptidase I and Arg-C proteinase digestion. The peptides were subjected to LC-MS analysis at Proteomic and

Metabolic core facility of MD Anderson Cancer Center. The numbers of peptides recovered from LiP-MS for each sample were normalized using only IL15 wild-type. Number of peptides recovered from LiP-MS is shown.

Computational modeling of *SNORD46*-IL15 Interaction—The Secondary structures of snoRNAs were predicted using RNAfold webserver[54]. The minimum free energy structure was selected for further investigation. The 3D structure of snoRNAs were predicted using Rosetta software[55]. The computational RNA structure models with highest scores will be used for the RNA-Protein docking studies. The crystal structure of IL15 was retrieved from the protein data bank (PDB ID: 2Z3Q). Protein preparation and energy minimization were processed using Schrodinger software suite. Then we performed RNA-Protein docking studies using multiple webservers including HDOCK[20], 3dRPC[21], and NPDock[22]. The binding poses with best scores were selected for examination of detailed interactions. Visualization of the RNA-Protein structure complexes and generation of final figures were performed using PyMOL v2.4.

Animal metabolic studies—Whole-body composition parameters were measured in male or female *Snord46*[WT/WT] or *Snord46*[G11A/G11A] mice at age of 12-weeks old by Faxitron Specimen Radiography System (Faxitron X-Ray Corp., Wheeling, IL) to precisely measure total body fat and lean mass. Mice were housed in the Oxymax/CLAMS (The Columbus Instruments Comprehensive Lab Animal Monitoring System) metabolic cage system from Columbus Instruments for 4 days with ad libitum access to food and water. VCO_2, VO_2, RER, and activity were measured by the Oxymax system. CLAMS was used to record the food and water intake, O_2 consumption, CO_2 expenditure, and energy expenditure. Mice (12-weeks old) were randomly grouped, and four mice were included in each group. Data reading and recording proceeded seven times per hour, and each mouse was housed and recorded for 72 h.

Tissue collection and immunohistochemistry (IHC)—Unless otherwise indicated, mice were fasted for 4-6 h, anesthetized with isoflurane, blood collected by heart puncture, and then sacrificed. Tissues were dissected, weighed, and either dipped in liquid nitrogen or fixed in 10% formalin solution. Pectoralis, triceps, quadriceps, gastrocnemius, and tibialis anterior muscles were dissected on one side of the body. The tissues fixed in formalin were processed and embedded in paraffin. The samples were sectioned into 4 μm thickness for the H&E, and IHC staining. Lipid droplet accumulation in the liver was visualized using Oil Red O (Millipore Sigma) staining of frozen liver sections prepared in an optimum cutting temperature (O.C.T.) compound (Fisher Scientific). Histopathology images were acquired with a light microscope (Olympus).

Blood analyses—Whole blood was collected by tail bleeding or cardiac puncture from mice fasted for 4-6 h. Total cholesterol (TC) and triglycerides (TG) were determined by enzymatic assays using commercial kits (BioAssay Systems). Alanine aminotransferase (ALT) and aspartate aminotransferase (AST) levels were measured using Alanine Transaminase Colorimetric Activity Assay Kit (Cayman Chemical) and EnzyChrom™ Aspartate Transaminase Assay Kit (BioAssay Systems). Serum levels of Leptin (R and D

Systems), Insulin (Thermo Fisher Scientific), and Ghrelin (Millipore Sigma) were measured by ELISA assay according to the manufacturer's instructions respectively.

Glucose and insulin tolerance tests—Insulin (ITT) and glucose (GTT) tolerance tests were performed on 6-h fasted male and female mice fed with chow or HFD. Glucose values were measured using the AimStrip® Plus Blood Glucose Meter (VWR, PA) by tail snip. Glucose (1g per kg body weight) and human insulin (0.75 U per kg body weight) were injected intraperitoneally (i.p.) after baseline glucose levels were measured in each mouse, and blood glucose levels were measured 15, 30, 45, 60, 90, and 120 min after injection.

Metabolic assays—Human adipocytes were cultured *in vitro*, and the cells and the supernatant were collected after the treatment with indicated cytokines. The intracellular NEFA and triglyceride were detected by Lipolysis Assay Kit (Zen-Bio) and Triglyceride Assay Kit (Zen-Bio) respectively. Extracellular/supernatant and serum NEFA were detected by Serum/Plasma Fatty Acid Detection Kit (Zen-Bio). OCR of adipocytes was measured using Seahorse XF Cell Mito Stress Test (Agilent Technologies). Briefly, human or mouse adipocytes were resuspended in XF assay media onto a XF24 cell plate pre-coated with Cell-Tak (Corning) followed by sequentially treatment with 1 μM oligomycin; 1 μM phenylhydrazone (FCCP); and 0.5 μM mixture including rotenone and antimycin A according to the instruction. Seahorse XFe Wave Software (Agilent) was applied to analyze the data.

Measurement of MGLL activity—MGLLL activity was measured as previously reported[56]. The reaction was set up in 200 ul assay buffer (10 mM Tris-HCl 1 mM EDTA pH 7.4, plus 0.1% fatty acid-free BSA) containing 25 ng of purified MGLL, 10 μM cold 2-arachidonoylglycerol (Cayman Chemical) and [^{3}H]-2-arachidonoylglycerol (American Radiolabeled Chemicals) as substrate at indicated concertation. The reaction mixture was incubated for 15 min at 37°C and then stopped by adding 400 μL of activated acid-washed charcoal). The contents were shaken at 37 °C for 90 seconds at 750 RPM, incubated at room temperature for 30 min, and then centrifuged at 2,000 x g for 10 min at room temperature. The 40 ul of aqueous phase was removed and combined with 160 ul of Ultima Gold scintillation liquid (PerkinElmer). Samples were then counted using a Beckman LS 6500 scintillation counter to measure the amount of [^{3}H]-glycerol in the supernatant cocktail (CPMs). The CPMs were converted to uM/min/mg protein based on a [^{3}H]-glycerol standard curve using MasterPlex® curve fitting software (Hitachi Solutions America). The MGLL activity (k_{cat})was calculated by Michaelis-Menten model using GraphPad Prism 9 software.

Assay of fatty acid uptake—[^{3}H]-oleic acid metabolic flux assay adapted from previous studies[57,58] was used to evaluate the CD36 activity in human adipocytes. The CPMs of cell lysate were counted using a Beckman LS 6500 scintillation counter and converted to uM/min/mg protein based on a [^{3}H]-oleic acid standard curve using MasterPlex® curve fitting software (Hitachi Solutions America). The CD36 activity (k_{cat}) was calculated by Michaelis-Menten model using GraphPad Prism 9 software.

NK cell isolation, cell viability determination, bulk RNA sequencing and analysis—NK cells were isolated form human PBMC. Human PBMC from healthy donors

or donors with obesity were obtained from STEMCELL Technologies. PBMC cells were negatively selected using CD3 as marker, the CD3⁻ cells were further selected by using CD56 as the positive selective marker, according to manufacturer's instruction (STEMCELL Technologies). The CD3-CD56⁺ NK cells were used in the following experiments. The cell viability of NK cells was determined using Trypan Blue dye, and automated cell counter (Bio-Rad), with or without Tubeimoside I (TBM) at the indicated concentration. The percentage of live cells normalized by the number of total cells were shown. Bulk RNA seq were performed by Novogene. RNAseq raw output fastq files were mapped to human transcriptome (genome version GENCODE v35, hg38) using Salmon (version 0.14.1), STAR2 (version 2.6.0b), and htseq (version 0.11.0) to produce raw gene counts and log2 transformed TPM reads. Differential gene expression was performed using raw counts and R DESeq2 package and results confirmed using TPM and R limma package. Pathway analyses were performed using GSEA and IPA software. Raw data and processed gene expression table were deposited to GEO (**GSE213465**).

Immunofluorescence and mIHC staining—IF staining was performed using NK cells isolated from human PBMC of healthy donors or donors with obesity. The cells were fixed with 4% paraformaldehyde solution and immune labeled using antibodies listed in the Table S6. The images were visualized with a Zeiss Axioskop2 Plus microscope. All immunostained slides were scanned on the APERIO ScanScope XT (Leica Biosystems) for quantification by digital image analysis. The quantification of IF staining density was performed by Image-Pro Plus 6.0 software (Media Cybernetics) and calculated based on the average staining intensity and the percentage of positively stained cells. For mIHC staining, formalin-fixed, paraffin-embedded (FFPE) tissue sections were cut at a thickness of 4 μm using a HistoCore BIOCUT Manual Rotary Microtome (Leica Biosystems). Staining of the sections with indicated antibodies was conducted using Opal™ Polaris 7 Color Automation IHC Detection Kit (Akoya Biosciences) and imaged with a PE Vectra Polaris Automated Quantitative Pathology Imaging System (PerkinElmer).

Flow cytometry—Cells were stained with various antibodies (Table S6) at room temperature for 15 min, washed with PBS and then re-suspended in PBS containing 1:200 dilution of Zombie Violet fixable viability dyes (BioLegend). Cells were then incubated for 15 min under room temperature and were fixed with 1.5% formaldehyde for 20 min under room temperature, washed one time and resuspended in FACS buffer (PBS with 5% fetal calf serum) before analysis on flow cytometer. Flow cytometry was performed on an LSR II system (BD Biosciences), and data were analyzed using FlowJo software (BD Biosciences).

CAR-NK cell generation and *in vitro* cytotoxicity—The hiPS cells derived from male donor were transfected with a CD133-CAR and the hiPS cells derived from female donor were transfected with an EGFR CAR. The CAR-iPS cells were then differentiated to NK cells by using the STEMdiff™ NK Cell Kit (STEMCELL Technologies). In brief, the CAR-iPS cells were induced to generate embryoid bodies for downstream lymphoid differentiation, after a total of 12 days culture, then CD34⁺ cells are enriched by EasySep™ positive selection. Then the hiPS-derived CD34⁺ cells were cultured in StemSpan™ Lymphoid Progenitor Expansion Medium for 14 days, followed by 14 days of culture using

StemSpan™ NK Cell Generation Kit to generate $CD56^+$ NK cells. Cells were harvested and analyzed for CD56, NKp46, NKp44, NKp30, NKG2D, and KIR expression by flow cytometry. MDA-MB-231 or HT-29 were incubated with EGFR-CAR-iPS-NK or CD133-CAR-iPS-NK cells at the 8:1 ratio in triplicate wells of U-bottomed 96-well plates. Target cell death was detected 6 h later by adding YOYO™-1 Iodide (491/509) (Thermo Fisher Scientific). The YOYO staining intensities were scanned on the APERIO ScanScope XT (Leica Biosystems) for quantification by digital image analysis. The quantification of IF staining density was performed by Image-Pro Plus 6.0 software (Media Cybernetics) and calculated based on the average staining intensity and the percentage of positively stained cells.

CAR-NK cell target tumorigenesis studies—6-8 weeks-old female NSG (NOD.Cg-*Prkdcscid Il2rgtm1Wjl*/SzJ, Jackson Laboratory) were raised under specific pathogen-free conditions. Animals were grouped randomly, and 3-5 mice were put into each cage. NSG mice under both chow and HFD-fed conditions were inoculated with $5×10^6$ MDA-MB231 cells orthotopically into the mammary fat pad, or $5×10^5$ HT-29 cells were implanted subcutaneously. Scramble or *Snord46* power inhibitors (10 mg/kg/day, IP injection) were administrated when tumor cells inoculation. EGFR-CAR-iPS-NK or CD133-CAR-iPS-NK $(1×10^7)$ cells were injected intravenously (every 7 days, 3 times in total) to tumor-bearing mice when tumor volume reached approximately 50 mm^3. Tumor size was measured every 4 days using a caliper, and tumor volume was calculated using the standard formula: $0.54×L×W^2$, where L is the longest diameter and W is the shortest diameter.

Quantification and statistical analysis—The experiment was set up to use 3-8 samples/repeats *per* experiment/group/condition to detect a 2-fold difference with power of 80% and at the significance level of 0.05 by a two-sided test for significant studies. Each of these experiments was independently repeated 3-5 times. Results were reported as mean ± standard deviation (SD) of at least three independent experiments, as indicated by figure legends. Each exact *n* value was indicated in the corresponding figure legend. Statistical analysis was performed using GraphPad Prism 9 software. Comparisons were analyzed by unpaired Student's *t*-test or one-way ANOVA test (n.s., $p > 0.05$, $*p < 0.05$, $**p < 0.01$, $***p < 0.001$ and $****p < 0.0001$), as indicated in individual figures. For survival analysis, Kaplan-Meier survival curves were compared using the log rank test.

Supplementary Material

Refer to Web version on PubMed Central for supplementary material.

Acknowledgements

Inclusion and diversity

We support inclusive, diverse, and equitable conduct of research.

References

1. Hales CM, Carroll MD, Fryar CD, and Ogden CL (2017). Prevalence of Obesity Among Adults and Youth: United States, 2015-2016. NCHS Data Brief, 1–8.

2. Berrington de Gonzalez A, Hartge P, Cerhan JR, Flint AJ, Hannan L, MacInnis RJ, Moore SC, Tobias GS, Anton-Culver H, Freeman LB, et al. (2010). Body-mass index and mortality among 1.46 million white adults. N Engl J Med 363, 2211–2219. 10.1056/NEJMoa1000367. [PubMed: 21121834]

3. Ringel AE, Drijvers JM, Baker GJ, Catozzi A, Garcia-Canaveras JC, Gassaway BM, Miller BC, Juneja VR, Nguyen TH, Joshi S, et al. (2020). Obesity Shapes Metabolism in the Tumor Microenvironment to Suppress Anti-Tumor Immunity. Cell 183, 1848–1866 e1826. 10.1016/j.cell.2020.11.009. [PubMed: 33301708]

4. Ma A, Koka R, and Burkett P (2006). Diverse functions of IL-2, IL-15, and IL-7 in lymphoid homeostasis. Annu Rev Immunol 24, 657–679. 10.1146/annurev.immunol.24.021605.090727. [PubMed: 16551262]

5. Barra NG, Reid S, MacKenzie R, Werstuck G, Trigatti BL, Richards C, Holloway AC, and Ashkar AA (2010). Interleukin-15 contributes to the regulation of murine adipose tissue and human adipocytes. Obesity (Silver Spring) 18, 1601–1607. 10.1038/oby.2009.445. [PubMed: 20019685]

6. Alvarez B, Carbo N, Lopez-Soriano J, Drivdahl RH, Busquets S, Lopez-Soriano FJ, Argiles JM, and Quinn LS (2002). Effects of interleukin-15 (IL-15) on adipose tissue mass in rodent obesity models: evidence for direct IL-15 action on adipose tissue. Biochim Biophys Acta 1570, 33–37. 10.1016/s0304-4165(02)00148-4. [PubMed: 11960686]

7. Ahmad A, Uddin S, and Steinhoff M (2020). CAR-T Cell Therapies: An Overview of Clinical Studies Supporting Their Approved Use against Acute Lymphoblastic Leukemia and Large B-Cell Lymphomas. Int J Mol Sci 21. 10.3390/ijms21113906.

8. Xia J, Minamino S, and Kuwabara K (2020). CAR-expressing NK cells for cancer therapy: a new hope. Biosci Trends 14, 354–359. 10.5582/bst.2020.03308. [PubMed: 32893255]

9. Tang F, Zhao LT, Jiang Y, Ba de N, Cui LX, and He W (2008). Activity of recombinant human interleukin-15 against tumor recurrence and metastasis in mice. Cell Mol Immunol 5, 189–196. 10.1038/cmi.2008.23. [PubMed: 18582400]

10. Yu P, Steel JC, Zhang M, Morris JC, and Waldmann TA (2010). Simultaneous blockade of multiple immune system inhibitory checkpoints enhances antitumor activity mediated by interleukin-15 in a murine metastatic colon carcinoma model. Clin Cancer Res 16, 6019–6028. 10.1158/1078-0432.CCR-10-1966. [PubMed: 20924130]

11. Robinson TO, and Schluns KS (2017). The potential and promise of IL-15 in immuno-oncogenic therapies. Immunol Lett 190, 159–168. 10.1016/j.imlet.2017.08.010. [PubMed: 28823521]

12. Liu E, Tong Y, Dotti G, Shaim H, Savoldo B, Mukherjee M, Orange J, Wan X, Lu X, Reynolds A, et al. (2018). Cord blood NK cells engineered to express IL-15 and a CD19-targeted CAR show long-term persistence and potent antitumor activity. Leukemia 32, 520–531. 10.1038/leu.2017.226. [PubMed: 28725044]

13. Steinbusch MM, Fang Y, Milner PI, Clegg PD, Young DA, Welting TJ, and Peffers MJ (2017). Serum snoRNAs as biomarkers for joint ageing and post traumatic osteoarthritis. Sci Rep 7, 43558. 10.1038/srep43558. [PubMed: 28252005]

14. Van Acker HH, Capsomidis A, Smits EL, and Van Tendeloo VF (2017). CD56 in the Immune System: More Than a Marker for Cytotoxicity? Front Immunol 8, 892. 10.3389/fimmu.2017.00892. [PubMed: 28791027]

15. Elkayam E, Kuhn CD, Tocilj A, Haase AD, Greene EM, Hannon GJ, and Joshua-Tor L (2012). The structure of human argonaute-2 in complex with miR-20a. Cell 150, 100–110. 10.1016/j.cell.2012.05.017. [PubMed: 22682761]

16. Feng Y, De Franceschi G, Kahraman A, Soste M, Melnik A, Boersema PJ, de Laureto PP, Nikolaev Y, Oliveira AP, and Picotti P (2014). Global analysis of protein structural changes in complex proteomes. Nat Biotechnol 32, 1036–1044. 10.1038/nbt.2999. [PubMed: 25218519]

17. Li Y, Tan Z, Zhang Y, Zhang Z, Hu Q, Liang K, Jun Y, Ye Y, Li YC, Li C, et al. (2021). A noncoding RNA modulator potentiates phenylalanine metabolism in mice. Science 373, 662–673. 10.1126/science.aba4991. [PubMed: 34353949]

18. Collins L, Tsien WH, Seals C, Hakimi J, Weber D, Bailon P, Hoskings J, Greene WC, Toome V, and Ju G (1988). Identification of specific residues of human interleukin 2 that affect binding to the 70-kDa subunit (p70) of the interleukin 2 receptor. Proc Natl Acad Sci U S A 85, 7709–7713. 10.1073/pnas.85.20.7709. [PubMed: 3051003]

19. Pettit DK, Bonnert TP, Eisenman J, Srinivasan S, Paxton R, Beers C, Lynch D, Miller B, Yost J, Grabstein KH, and Gombotz WR (1997). Structure-function studies of interleukin 15 using site-specific mutagenesis, polyethylene glycol conjugation, and homology modeling. J Biol Chem 272, 2312–2318. 10.1074/jbc.272.4.2312. [PubMed: 8999939]

20. Yan Y, Zhang D, Zhou P, Li B, and Huang SY (2017). HDOCK: a web server for protein-protein and protein-DNA/RNA docking based on a hybrid strategy. Nucleic Acids Res 45, W365–W373. 10.1093/nar/gkx407. [PubMed: 28521030]

21. Huang Y, Li H, and Xiao Y (2018). 3dRPC: a web server for 3D RNA-protein structure prediction. Bioinformatics 34, 1238–1240. 10.1093/bioinformatics/btx742. [PubMed: 29186336]

22. Tuszynska I, Magnus M, Jonak K, Dawson W, and Bujnicki JM (2015). NPDock: a web server for protein-nucleic acid docking. Nucleic Acids Res 43, W425–430. 10.1093/nar/gkv493. [PubMed: 25977296]

23. Lacraz G, Rakotoarivelo V, Labbe SM, Vernier M, Noll C, Mayhue M, Stankova J, Schwertani A, Grenier G, Carpentier A, et al. (2016). Deficiency of Interleukin-15 Confers Resistance to Obesity by Diminishing Inflammation and Enhancing the Thermogenic Function of Adipose Tissues. PLoS One 11, e0162995. 10.1371/journal.pone.0162995. [PubMed: 27684068]

24. Klok MD, Jakobsdottir S, and Drent ML (2007). The role of leptin and ghrelin in the regulation of food intake and body weight in humans: a review. Obes Rev 8, 21–34. 10.1111/j.1467-789X.2006.00270.x. [PubMed: 17212793]

25. Kojima M, Hosoda H, Date Y, Nakazato M, Matsuo H, and Kangawa K (1999). Ghrelin is a growth-hormone-releasing acylated peptide from stomach. Nature 402, 656–660. 10.1038/45230. [PubMed: 10604470]

26. Calderon-Dominguez M, Mir JF, Fucho R, Weber M, Serra D, and Herrero L (2016). Fatty acid metabolism and the basis of brown adipose tissue function. Adipocyte 5, 98–118. 10.1080/21623945.2015.1122857. [PubMed: 27386151]

27. Rosen ED, and Spiegelman BM (2014). What we talk about when we talk about fat. Cell 156, 20–44. 10.1016/j.cell.2013.12.012. [PubMed: 24439368]

28. Nomura DK, Long JZ, Niessen S, Hoover HS, Ng SW, and Cravatt BF (2010). Monoacylglycerol lipase regulates a fatty acid network that promotes cancer pathogenesis. Cell 140, 49–61. 10.1016/j.cell.2009.11.027. [PubMed: 20079333]

29. Tran TT, Poirier H, Clement L, Nassir F, Pelsers MM, Petit V, Degrace P, Monnot MC, Glatz JF, Abumrad NA, et al. (2011). Luminal lipid regulates CD36 levels and downstream signaling to stimulate chylomicron synthesis. J Biol Chem 286, 25201–25210. 10.1074/jbc.M111.233551. [PubMed: 21610069]

30. Elaraby E, Malek AI, Abdullah HW, Elemam NM, Saber-Ayad M, and Talaat IM (2021). Natural Killer Cell Dysfunction in Obese Patients with Breast Cancer: A Review of a Triad and Its Implications. J Immunol Res 2021, 9972927. 10.1155/2021/9972927. [PubMed: 34212054]

31. Michelet X, Dyck L, Hogan A, Loftus RM, Duquette D, Wei K, Beyaz S, Tavakkoli A, Foley C, Donnelly R, et al. (2018). Metabolic reprogramming of natural killer cells in obesity limits antitumor responses. Nat Immunol 19, 1330–1340. 10.1038/s41590-018-0251-7. [PubMed: 30420624]

32. Feng X, Zhou J, Li J, Hou X, Li L, Chen Y, Fu S, Zhou L, Li C, and Lei Y (2018). Tubeimoside I induces accumulation of impaired autophagolysosome against cervical cancer cells

by both initiating autophagy and inhibiting lysosomal function. Cell Death Dis 9, 1117. 10.1038/s41419-018-1151-3. [PubMed: 30389907]

33. Xia L, Zheng ZZ, Liu JY, Chen YJ, Ding JC, Xia NS, Luo WX, and Liu W (2020). EGFR-targeted CAR-T cells are potent and specific in suppressing triple-negative breast cancer both in vitro and in vivo. Clin Transl Immunology 9, e01135. 10.1002/cti2.1135. [PubMed: 32373345]

34. Yu S, Li A, Liu Q, Li T, Yuan X, Han X, and Wu K (2017). Chimeric antigen receptor T cells: a novel therapy for solid tumors. J Hematol Oncol 10, 78. 10.1186/s13045-017-0444-9. [PubMed: 28356156]

35. Wang Y, Chen M, Wu Z, Tong C, Dai H, Guo Y, Liu Y, Huang J, Lv H, Luo C, et al. (2018). CD133-directed CAR T cells for advanced metastasis malignancies: A phase I trial. Oncoimmunology 7, e1440169. 10.1080/2162402X.2018.1440169. [PubMed: 29900044]

36. Vora P, Venugopal C, Salim SK, Tatari N, Bakhshinyan D, Singh M, Seyfrid M, Upreti D, Rentas S, Wong N, et al. (2020). The Rational Development of CD133-Targeting Immunotherapies for Glioblastoma. Cell Stem Cell 26, 832–844 e836. 10.1016/j.stem.2020.04.008. [PubMed: 32464096]

37. Nielsen AR, Hojman P, Erikstrup C, Fischer CP, Plomgaard P, Mounier R, Mortensen OH, Broholm C, Taudorf S, Krogh-Madsen R, et al. (2008). Association between interleukin-15 and obesity: interleukin-15 as a potential regulator of fat mass. J Clin Endocrinol Metab 93, 4486–4493. 10.1210/jc.2007-2561. [PubMed: 18697873]

38. Febbraio MA (2014). Role of interleukins in obesity: implications for metabolic disease. Trends Endocrinol Metab 25, 312–319. 10.1016/j.tem.2014.02.004. [PubMed: 24698032]

39. Quinn LS, Anderson BG, Strait-Bodey L, Stroud AM, and Argiles JM (2009). Oversecretion of interleukin-15 from skeletal muscle reduces adiposity. Am J Physiol Endocrinol Metab 296, E191–202. 10.1152/ajpendo.90506.2008. [PubMed: 19001550]

40. Carbo N, Lopez-Soriano J, Costelli P, Alvarez B, Busquets S, Baccino FM, Quinn LS, Lopez-Soriano FJ, and Argiles JM (2001). Interleukin-15 mediates reciprocal regulation of adipose and muscle mass: a potential role in body weight control. Biochim Biophys Acta 1526, 17–24. 10.1016/s0304-4165(00)00188-4. [PubMed: 11287118]

41. Taschler U, Radner FP, Heier C, Schreiber R, Schweiger M, Schoiswohl G, Preiss-Landl K, Jaeger D, Reiter B, Koefeler HC, et al. (2011). Monoglyceride lipase deficiency in mice impairs lipolysis and attenuates diet-induced insulin resistance. J Biol Chem 286, 17467–17477. 10.1074/jbc.M110.215434. [PubMed: 21454566]

42. Dione N, Lacroix S, Taschler U, Deschenes T, Abolghasemi A, Leblanc N, Di Marzo V, and Silvestri C (2020). Mgll Knockout Mouse Resistance to Diet-Induced Dysmetabolism Is Associated with Altered Gut Microbiota. Cells 9. 10.3390/cells9122705.

43. Labar G, Bauvois C, Borel F, Ferrer JL, Wouters J, and Lambert DM (2010). Crystal structure of the human monoacylglycerol lipase, a key actor in endocannabinoid signaling. Chembiochem 11, 218–227. 10.1002/cbic.200900621. [PubMed: 19957260]

44. Febbraio M, Abumrad NA, Hajjar DP, Sharma K, Cheng W, Pearce SF, and Silverstein RL (1999). A null mutation in murine CD36 reveals an important role in fatty acid and lipoprotein metabolism. J Biol Chem 274, 19055–19062. 10.1074/jbc.274.27.19055. [PubMed: 10383407]

45. Chu J, Xing C, Du Y, Duan T, Liu S, Zhang P, Cheng C, Henley J, Liu X, Qian C, et al. (2021). Pharmacological inhibition of fatty acid synthesis blocks SARS-CoV-2 replication. Nat Metab 3, 1466–1475. 10.1038/s42255-021-00479-4. [PubMed: 34580494]

46. Buganova M, Pelantova H, Holubova M, Sediva B, Maletinska L, Zelezna B, Kunes J, Kacer P, Kuzma M, and Haluzik M (2017). The effects of liraglutide in mice with diet-induced obesity studied by metabolomics. J Endocrinol 233, 93–104. 10.1530/JOE-16-0478. [PubMed: 28138003]

47. Hemmrich K, von Heimburg D, Cierpka K, Haydarlioglu S, and Pallua N (2005). Optimization of the differentiation of human preadipocytes in vitro. Differentiation 73, 28–35. 10.1111/j.1432-0436.2005.07301003.x. [PubMed: 15733065]

48. Lee JY, Sohn KH, Rhee SH, and Hwang D (2001). Saturated fatty acids, but not unsaturated fatty acids, induce the expression of cyclooxygenase-2 mediated through Toll-like receptor 4. J Biol Chem 276, 16683–16689. 10.1074/jbc.M011695200. [PubMed: 11278967]

49. Joshi-Barve S, Barve SS, Amancherla K, Gobejishvili L, Hill D, Cave M, Hote P, and McClain CJ (2007). Palmitic acid induces production of proinflammatory cytokine interleukin-8 from hepatocytes. Hepatology 46, 823–830. 10.1002/hep.21752. [PubMed: 17680645]

50. Fey A, Eichler S, Flavier S, Christen R, Hofle MG, and Guzman CA (2004). Establishment of a real-time PCR-based approach for accurate quantification of bacterial RNA targets in water, using Salmonella as a model organism. Appl Environ Microbiol 70, 3618–3623. 10.1128/AEM.70.6.3618-3623.2004. [PubMed: 15184165]

51. Dejardin J, and Kingston RE (2009). Purification of proteins associated with specific genomic Loci. Cell 136, 175–186. 10.1016/j.cell.2008.11.045. [PubMed: 19135898]

52. Zhang Y, Li Y, Hu Q, Xi Y, Xing Z, Zhang Z, Huang L, Wu J, Liang K, Nguyen TK, et al. (2020). The lncRNA H19 alleviates muscular dystrophy by stabilizing dystrophin. Nat Cell Biol 22, 1332–1345. 10.1038/s41556-020-00595-5. [PubMed: 33106653]

53. Jensen KB, and Darnell RB (2008). CLIP: crosslinking and immunoprecipitation of in vivo RNA targets of RNA-binding proteins. Methods Mol Biol 488, 85–98. 10.1007/978-1-60327-475-3_6. [PubMed: 18982285]

54. Gruber AR, Lorenz R, Bernhart SH, Neubock R, and Hofacker IL (2008). The Vienna RNA websuite. Nucleic Acids Res 36, W70–74. 10.1093/nar/gkn188. [PubMed: 18424795]

55. Watkins AM, Rangan R, and Das R (2020). FARFAR2: Improved De Novo Rosetta Prediction of Complex Global RNA Folds. Structure 28, 963–976 e966. 10.1016/j.str.2020.05.011. [PubMed: 32531203]

56. Douglass JD, Zhou YX, Wu A, Zadroga JA, Gajda AM, Lackey AI, Lang W, Chevalier KM, Sutton SW, Zhang SP, et al. (2015). Global deletion of MGL in mice delays lipid absorption and alters energy homeostasis and diet-induced obesity. J Lipid Res 56, 1153–1171. 10.1194/jlr.M058586. [PubMed: 25842377]

57. Stremmel W (1988). Uptake of fatty acids by jejunal mucosal cells is mediated by a fatty acid binding membrane protein. J Clin Invest 82, 2001–2010. 10.1172/JCI113820. [PubMed: 3198762]

58. Hao JW, Wang J, Guo H, Zhao YY, Sun HH, Li YF, Lai XY, Zhao N, Wang X, Xie C, et al. (2020). CD36 facilitates fatty acid uptake by dynamic palmitoylation-regulated endocytosis. Nat Commun 11, 4765. 10.1038/s41467-020-18565-8. [PubMed: 32958780]
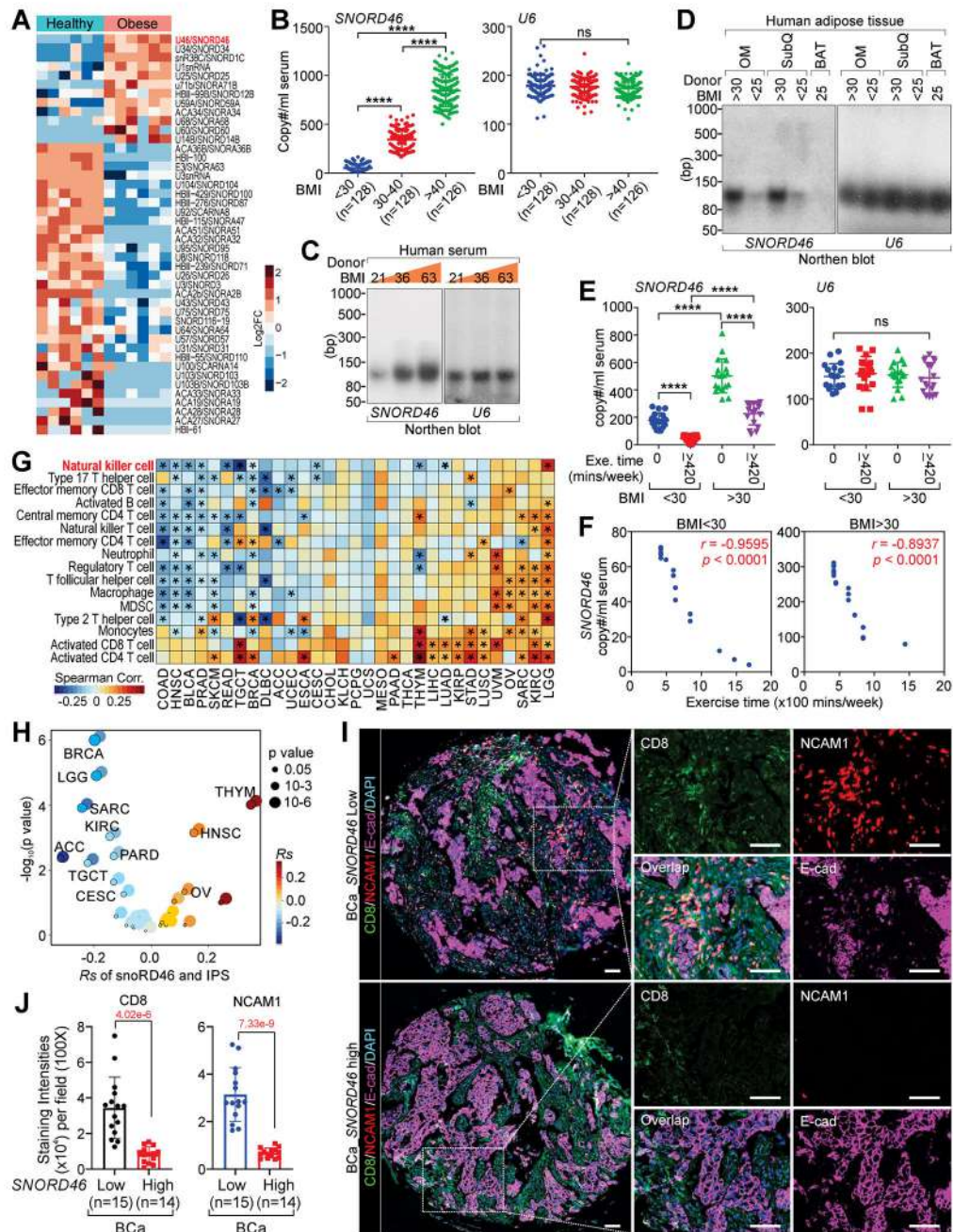
Figure 1. *SNORD46* correlates with BMI and immune resistance

(**A**) Heatmap of snoRNA expression of indicated human serum samples.

(**B**) Copy number of *SNORD46* (left) or *U6* (right) in serum of human donors with BMI < 25, 30-40, or > 40 (n = 128, 128, 126 donors).

(**C and D**) Northern blotting using indicated probes of indicated human serum (C), or human adipose tissues as indicated (D).

(**E**) Copy number of *SNORD46* (left) or *U6* (right) in serum with indicated BMI, without or with exercise (0, 420 min/week), n = 18 donor per group, one-way ANOVA.

(**F**) Pearson correlation between *SNORD46* copy number and exercise time of donors with BMI < 30 (left) or BMI > 30 (right), n = 18 (BMI < 30), 18 (BMI > 30) donor, Fisher's exact test.

(**G** and **H**) The spearman's correlation of *SNORD46* expression and immune cell type enrichment (G) and immunophenoscore (IPS) (H) in 28 cancer types.

(**I** and **J**) Representative multi-IHC images (I) and statistical analysis of CD8 and NCAM1 (J) of breast cancer tissues from serum *SNORD46*-high or *SNORD46*-low breast cancer patients. Scale bars, 100 μm. Error bars, SD, n = 15, 14 tissues, unpaired Student's t-test.
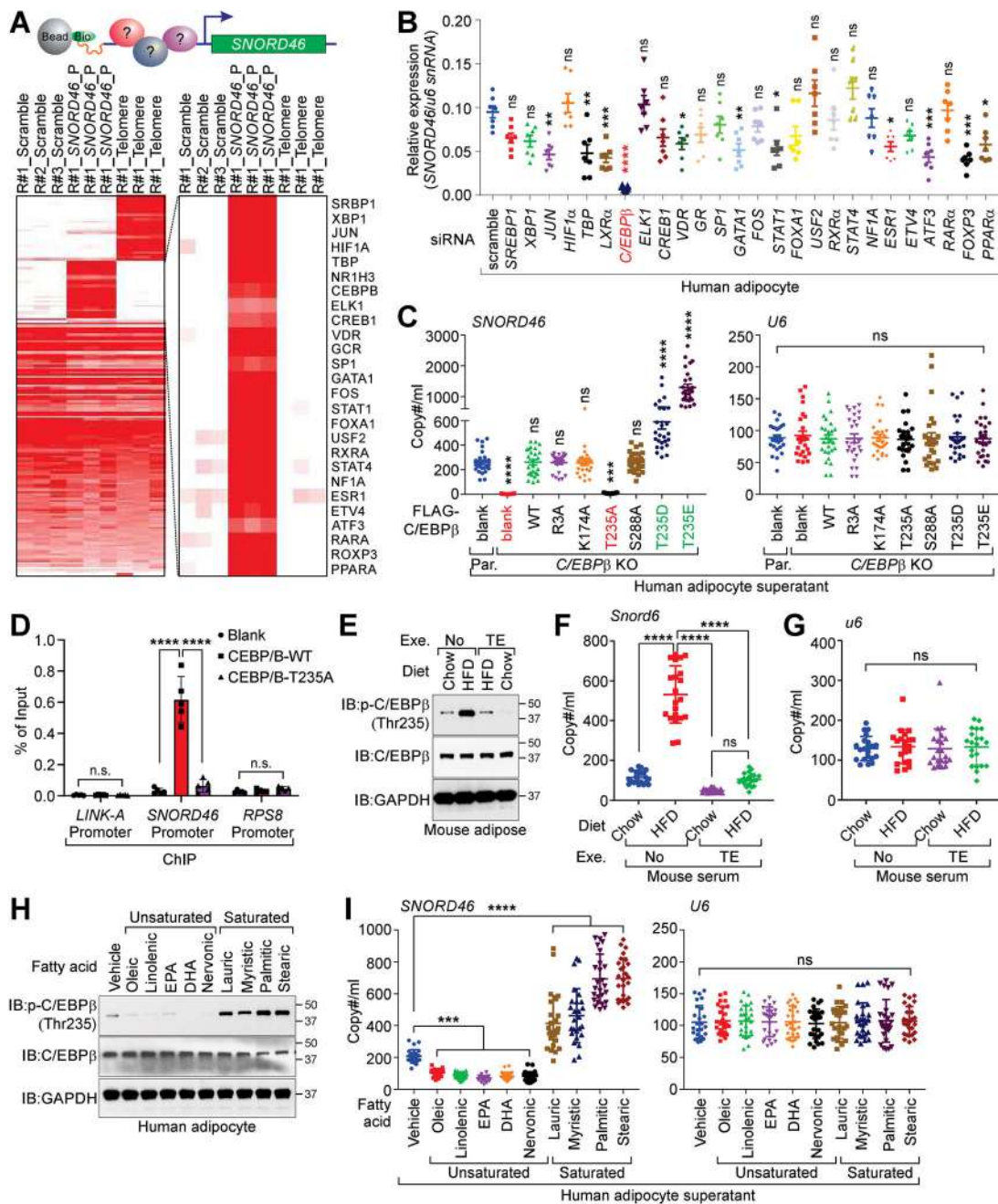
Figure 2. C/EBPβ regulates the transcriptional expression of *SNORD46*

(**A**) Top: graphic illustration of PICh-MS determination using *SNORD46* promoter region. Bottom: heatmap of the PICh-MS protein identification using scramble, *SNORD46* promoter or telomere sequence as indicated. R: biological repeat.

(**B**) Relative expression of *SNORD46*, normalized by *U6* snRNA of differentiated human adipocyte harboring indicated siRNAs. Error bars, SD, n = 7 independent experiments, one-way ANOVA.

(**C**) Copy number of *SNORD46* (left) or *U6* (right) in supernatant of C/EBPβ parental (Par.) or knockout (KO) adipocytes expressing indicated expression vectors. Error bars, SD, n = 26 donors, one-way ANOVA.

(**D**) ChIP-qPCR detection of the C/EBPβ occupancy on *LINK-A*, *SNORD46* or *RPS8* promoter regions of differentiated human adipocytes expressing indicated expression constructs. Error bars, SD, n = 5 independent experiments, two-way ANOVA.

(**E**) Immunoblotting (IB) detection of indicated proteins in adipose tissues from chow or HFD-fed mice with or without treadmill exercise (TE).

(**F** and **G**) Serum *Snord46* (F) or *U6* (G) copy number in wild-type mice challenged with chow or HFD followed with or without treadmill exercise. Error bars, SD, n = 21 mice per group, one-way ANOVA.

(**H**) IB detection of indicated proteins in differentiated human adipocytes supernatant upon indicated stimuli.

(**I**) Copy number of *SNORD46* (left) or *U6* (right) in differentiated human adipocytes supernatant upon indicated stimuli. Error bars, SD, n = 26 donors, one-way ANOVA.
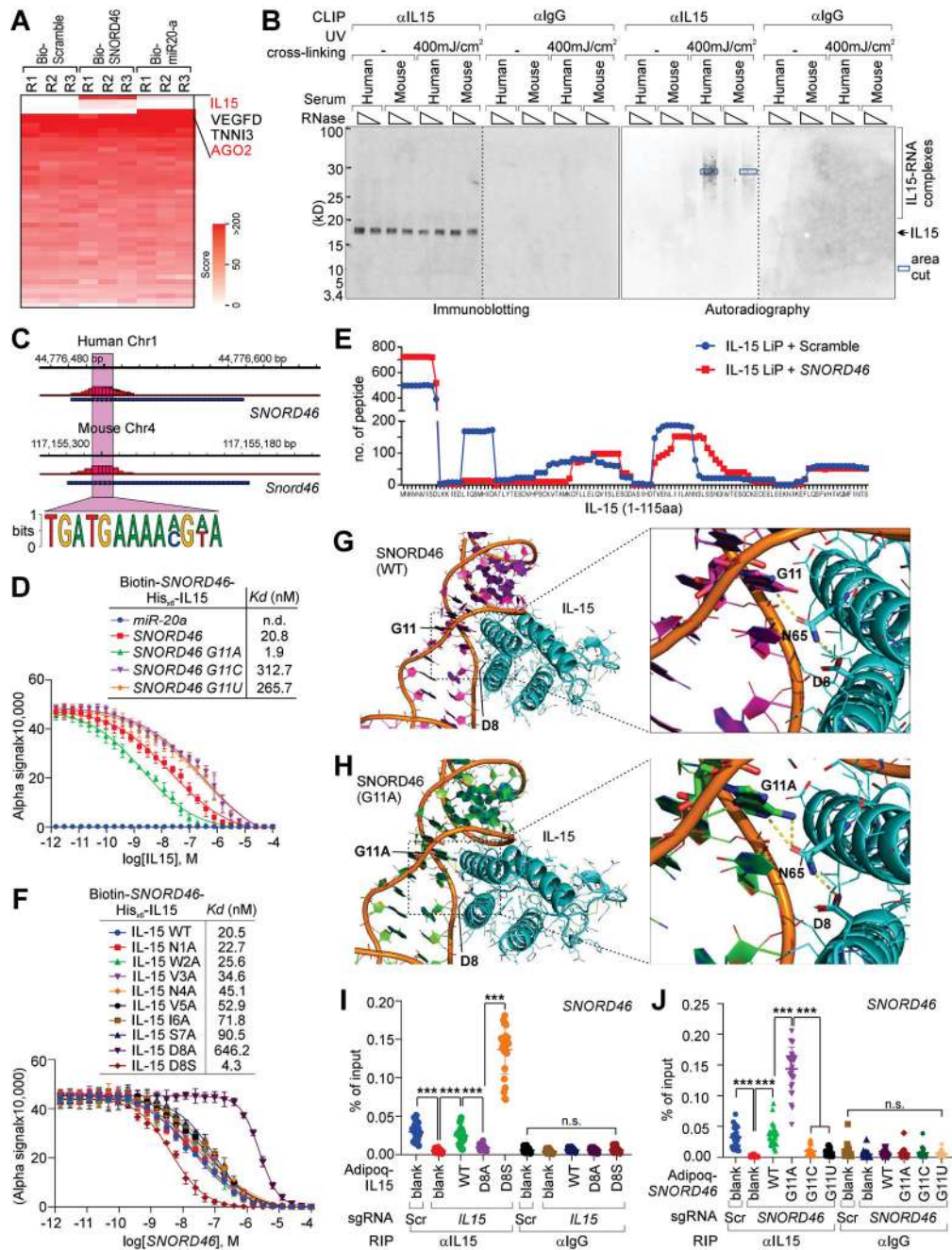
Figure 3. *SNORD46* physically interact with IL15

(**A**) Heatmap of the protein identification score for biotinylated Scramble, *SNORD46* or *miR-20a* pull-down. R: biological replicate.

(**B**) IB detection (left) and autoradiography (right) of IL15 CLIP assay using human (H) or mice (M) serum. Blue box: RNA-protein complex extracted for the following sanger sequencing.

(**C**) Summary of *SNORD46* sequence responsible for IL15 binding. The chromatin sequences corresponding to RNA (negative-stranded) and RNA motif bound by IL15 are shown.

(**D**) Competition binding assay to determine K_d of the interaction between His-tagged IL15 and biotinylated-*SNORD46* wild-type or mutants. Unlabeled IL15 serve as the competitor. Error bars, SD, n = 3 independent experiments. *miR-20a* was included as a negative control.

(**E**) Number of peptides recovered from LiP-MS of IL15 incubated with scramble or *SNORD46* RNA. x-axis: amino acid position of full-length IL15.

(**F**) Competition binding assay to determine K_d of the interaction between His-tagged IL15 wild-type or mutants and biotinylated-*SNORD46*. Unlabeled *SNORD46* serve as competitor. Error bars, SD, n = 3 independent experiments.

(**G**) Computational modeling of *SNORD46*–IL15 interaction. Magenta cartoon: *SNORD46*; Cyan cartoon: IL15; Magenta stick: G11; Cyan stick: D8 and N65.

(**H**) G11A mutation of *SNORD46* strengthens the interaction with IL15. Green cartoon: *SNORD46*; Cyan cartoon: IL15; Green stick: A11; Cyan stick: D8 and N65.

(**I** and **J**) RIP assay using differentiated human adipocytes harboring IL15 sgRNAs (I), or *SNORD46* sgRNAs (J) and *Adipoq*-driven expression of indicated mutants. Error bars, SD, n = 26 donors, one-way ANOVA.
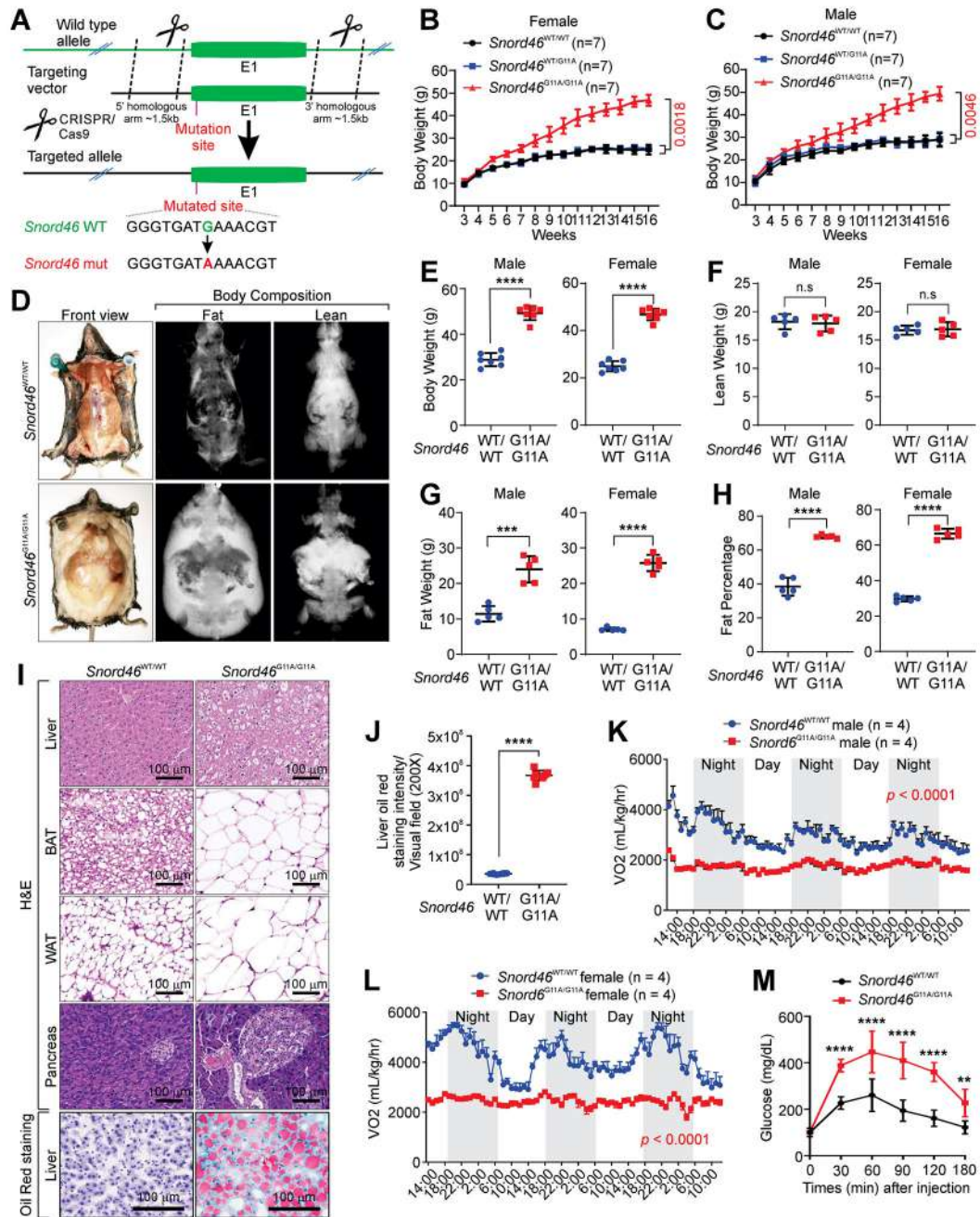
Figure 4. *SNORD46* G11A drives obesity

(**A**) Schematic of CRISPR-Cas9 method used to generate *SNORD46*$^{G11A/G11A}$ mice.

(**B** and **C**) Body weight measurement of female (B) or male (C) *Snord46*$^{WT/WT}$, *Snord46*$^{WT/G11A}$ or *Snord46*$^{G11A/G11A}$ mice. Error bars, SD, n = 7 mice, one-way ANOVA.

(**D-H**) Representative images of lean and fat tissues (D), quantification of male (left) or female (right) body weight (E), lean weight (F), fat weight (G), and fat percentage (H) by the dual energy x-ray absorptiometry imaging system from *Snord46*$^{WT/WT}$ or *Snord46*$^{G11A/G11A}$ mice. Error bars, SD, n = 5 mice, Student's t-test.

(**I**) Representative H&E and Oil Red O staining of indicated tissues from *Snord46*$^{WT/WT}$ or *Snord46*$^{G11A/G11A}$ mice. Scale bars, 100 μm.

(**J**) Statistical analysis of Oil Red O staining intensity of liver sections from *Snord46*$^{WT/WT}$ or *Snord46*$^{G11A/G11A}$ mice. Error bars, SD, n = 8 mice, Student's t-test.

(**K** and **L**) CLAMS measurement of oxygen consumption (VO_2) in male (**K**) or female (**L**) *Snord46*$^{WT/WT}$ or *Snord46*$^{G11A/G11A}$ mice. Error bars, SD, n = 4, 4 mice, two-way ANOVA.

(**M**) Glucose tolerance tests (GTTs) of male *Snord46*$^{WT/WT}$ or *Snord46*$^{G11A/G11A}$ mice at the indicated time points. Error bars, SD, n = 8, 5 mice, Student's t-test for each time point.
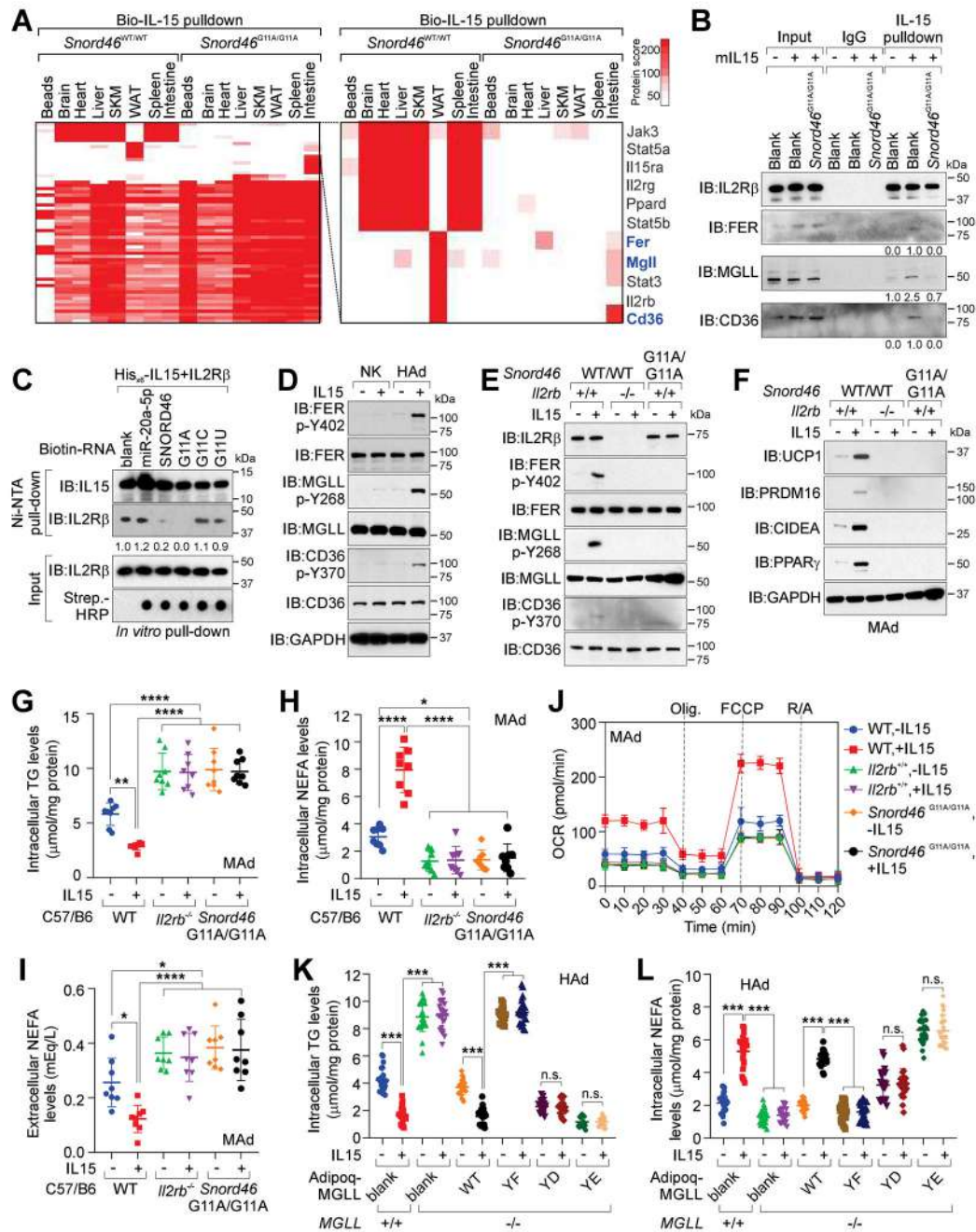
Figure 5. IL15 triggers FER-medicated signaling cascades in adipocytes to regulates the enzymatic activities of CD36 and MGLL

(**A**) Identification of biotinylated IL15-associated proteins in *Snord46*[WT/WT] or *Snord46*[G11A/G11A] tissues as indicated. Protein scores are shown.

(**B**) IL15 pull-down followed by IB detection of indicated proteins in mouse adipocytes with or without IL15 stimulation.

(**C**) Ni-NTA pull-down using indicated recombinant proteins and biotinylated RNA oligonucleotides, followed by IB detection using indicated antibodies.
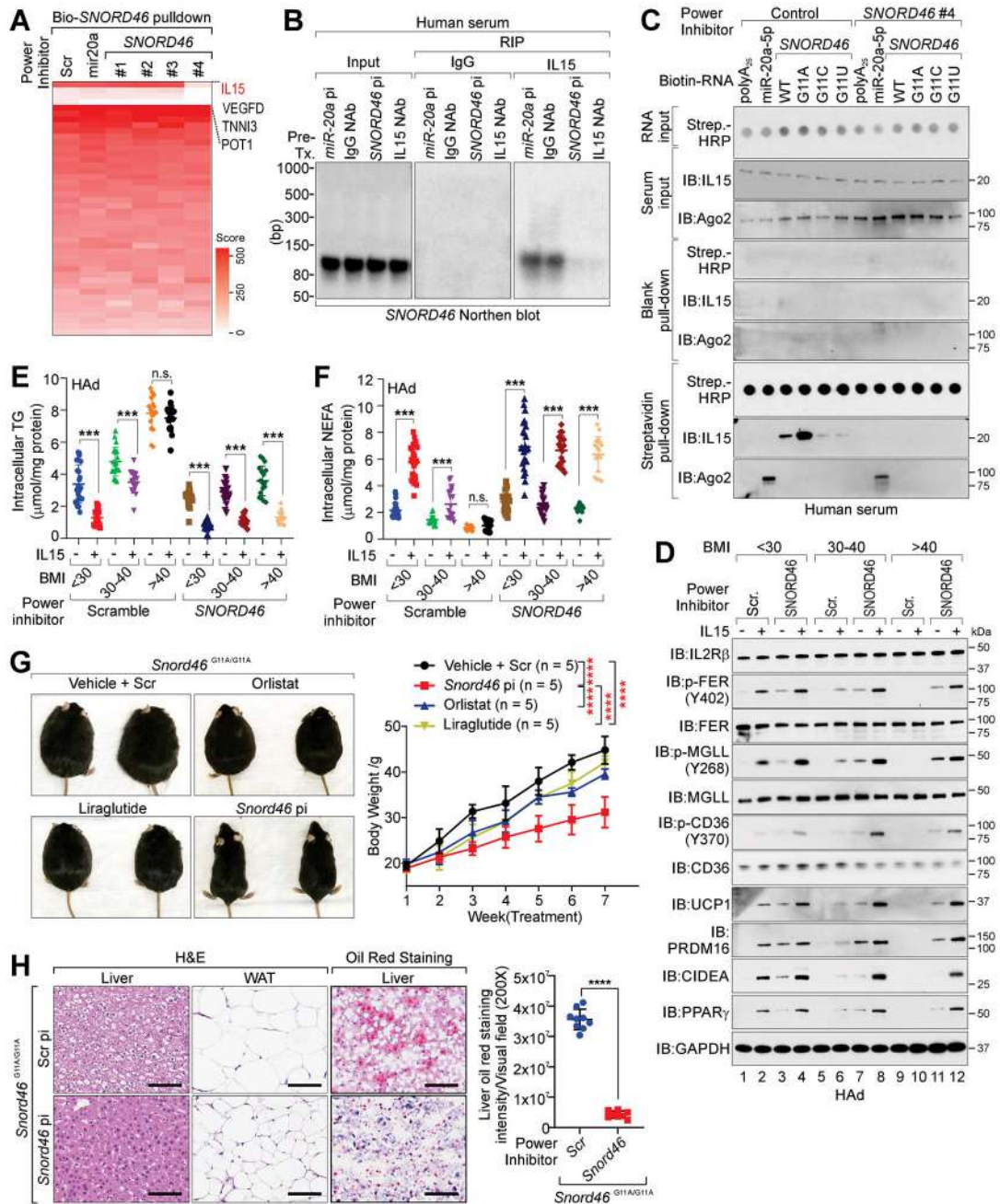
(**D**) IB detection of indicated proteins in NK cells or differentiated human adipocytes (HAd) with or without IL15 stimulation.

(**E** and **F**) IB detection of indicated proteins in WT, *Il2rb*-deficient or *Snord46*$^{G11A/G11A}$ adipocytes with or without IL15 stimulation.

(**G-I**) Measurement of intracellular TG (G), intracellular NEFA (H), or extracellular NEFA (I) concentration of differentiated WT, *Il2rb*$^{-/-}$or *Snord46*$^{G11A/G11A}$ adipocytes with or without IL15 stimulation. Error bars, SD, n = 8 animals per experimental group, one-way ANOVA.

(**J**) Oxygen consumption rate (OCR) across time for WT, *Il2rb*$^{-/-}$ and *Snord46*$^{G11A/G11A}$ mouse adipocytes with or without IL15 stimulation. Dot lines indicate the addition of mitochondrial inhibitors (oligomycin; FCCP; antimycin A/rotenone) (n = 8 wells of adipocytes, error bars: SD).

(**K** and **L**) Measurement of intracellular TG (K) and intracellular NEFA (L) levels in *MGLL*-proficient or -deficient differentiated human adipocytes expressing indicated expression constructs with or without IL15 stimulation. Error bars, SD, n = 24 donors, two-way ANOVA.

**Figure 6. *SNORD46* power inhibitors antagonize obesity**

(**A**) Heatmap of the protein identification score for biotinylated Scramble, *SNORD46* or *miR-20a* pull-down in the presence of indicated power inhibitors. R: biological replicate.

(**B**) Northernblot of *SNORD46* in human serum treated with indicated power inhibitors or antibodies.

(**C**) IB detection of proteins associated with biotinylated RNA (wild-type and indicated mutants) in human serum treated with indicated power inhibitors.

(**D**) IB detection of indicated proteins in differentiated human adipocytes collected from donors with BMI < 25, 30-40, or > 40 and treated with IL15 and/or indicated power inhibitors.

(**E** and **F**) Measurement of intracellular TG (E) or intracellular NEFA (F) levels in differentiated human adipocytes collected from donors with BMI < 25 (n = 24), 30-40 (n= 19), or > 40 (n = 17) and treated with indicated power inhibitors with or without IL15 stimulation. Error bars, SD, two-way ANOVA.

(**G**) Left, representative images; right, body weight measurement of $Snord46^{G11A/G11A}$ mice treated with scramble (Scr), $Snord46$ power inhibitor (pi), Orlistat or Liraglutide as indicated. Error bars, SD, n = 5 mice per group, one-way ANOVA.

(**H**) Representative H&E and Oil Red O staining of liver or WAT (left) and statistical analysis of staining intensities of liver sections (right) from $Snord46^{G11A/G11A}$ mice treated with scramble or $Snord46$ power inhibitor. Scale bars, 100 μm. Error bars, SD, n= 9, 8 mice, Student's t-test.
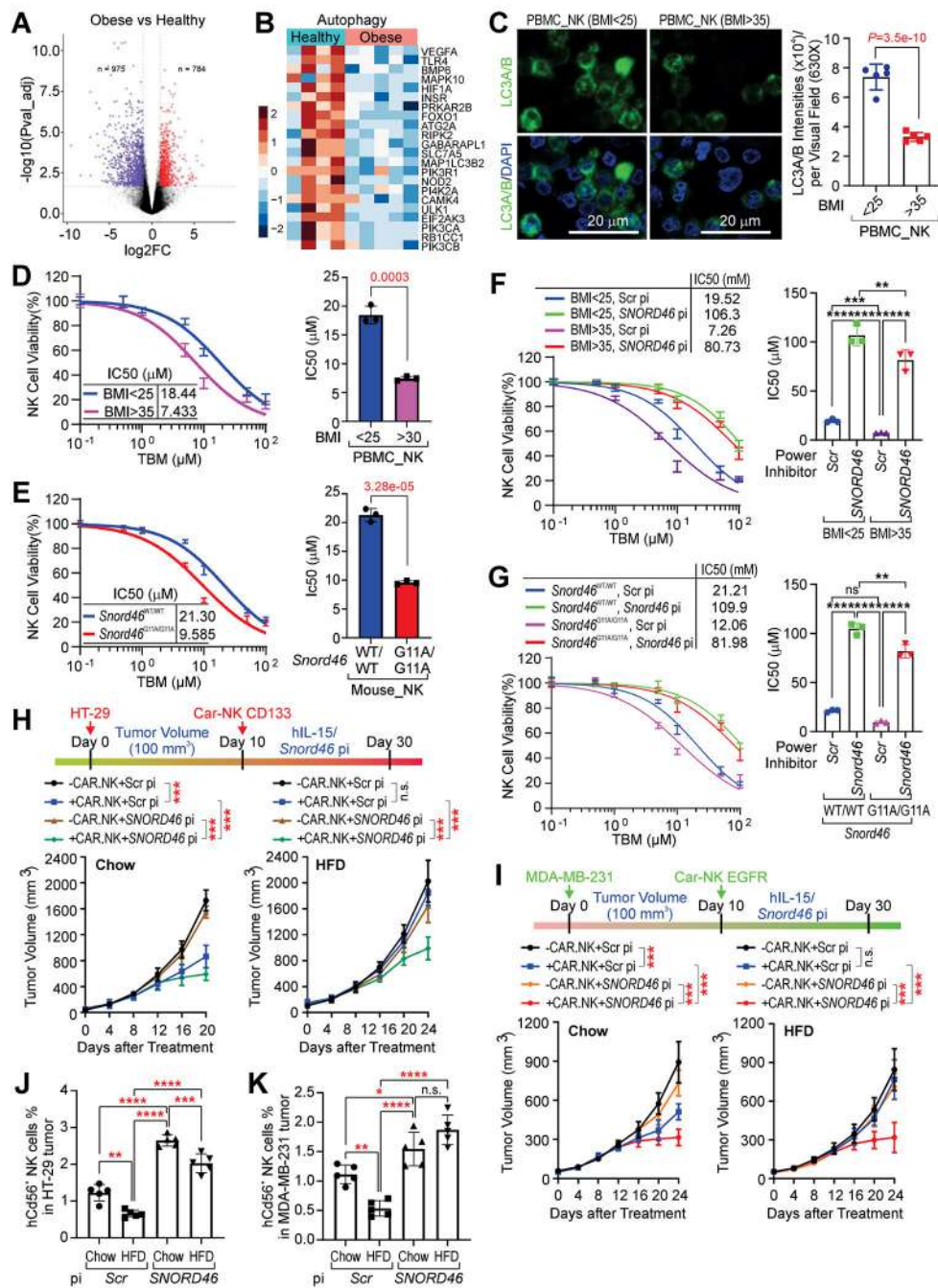
Figure 7. *SNORD46* power inhibitors restore the anti-tumor immunity of CAR-NK cells under obesity

(**A**) Volcano presentation of the transcription profiling of NK cells isolated from donors with obesity (n = 5) or healthy donors (n = 4).

(**B**) Heatmap of the expression of Autophagy gene signature of NK cells isolated from donors with obesity (n = 5) or healthy donors (n = 4).

(**C**) Immunofluorescent labeling using indicated antibodies in NK cells isolated from PBMC of healthy donors (BMI < 25) or donors with obesity (BMI > 35). Scale bars, 20 μm. Error bars, SD, n = 5, 5 donors, Student's t-test.

(**D**) Percentage of NK cells viability (left) and IC_{50} determination of NK cells viability (right) of BMI < 25, or BMI > 35 donors. Error bars, SD, n = 3 independent experiment, Student's t-test.

(**E**) Percentage of NK cells viability (left) and IC_{50} determination of NK cells viability (right) of *Snord46*$^{WT/WT}$ or *Snord46*$^{G11A/G11A}$ mice. Error bars, SD, n = 3 independent experiment, Student's t-test.

(**F**) Percentage of NK cells viability (left) and IC_{50} determination of NK cells viability (right) of BMI < 25, or BMI > 35 donors treated with scramble or *SNORD46* power inhibitor. Error bars, SD, n = 3 independent experiment, one-way ANOVA.

(**G**) Percentage of NK cells viability (left) and IC_{50} determination of NK cells viability (right) of *Snord46*$^{WT/WT}$ or *Snord46*$^{G11A/G11A}$ mice treated with scramble or *Snord46* power inhibitor. Error bars, SD, n = 3 independent experiment, one-way ANOVA.

(**H**) Top: schematic illustration of CAR-NK cells in HT-29 xenograft tumors. Bottom: tumor volume measurement of HT-29 tumor of chow (left) or HFD-fed animals (right) upon CAR-NK and indicated powder inhibitor treatment. Error bars, SD, n = 5 mice per group, one-way ANOVA.

(**I**) Top: schematic illustration of CAR-NK cells in MDA-MB-231 xenograft tumors. Bottom: tumor volume measurement of MDA-MB-231 tumor of chow (left) or HFD-fed animals (right) upon CAR-NK and indicated power inhibitor treatment. Error bars, SD, n = 5 mice per group, one-way ANOVA.

(**J** and **K**) Percentage of CD56$^+$ NK cells isolated from HT-29 tumor (J) or MDA-MB-231 tumor (K) of chow or HFD-fed animals upon indicated treatment. Error bars, SD, n = 5 mice per group, one-way ANOVA.